



## Six new epibiotic *Proschkinia* (Bacillariophyta) species and new insights into the genus phylogeny

Roksana Majewska, Sunčica Bosak, Thomas A. Frankovich, Matt P. Ashworth, Michael J. Sullivan, Nathan J. Robinson, Eric A. Lazo-Wasem, Theodora Pinou, Ronel Nel, Schonna R. Manning & Bart Van de Vijver

To cite this article: Roksana Majewska, Sunčica Bosak, Thomas A. Frankovich, Matt P. Ashworth, Michael J. Sullivan, Nathan J. Robinson, Eric A. Lazo-Wasem, Theodora Pinou, Ronel Nel, Schonna R. Manning & Bart Van de Vijver (2019) Six new epibiotic *Proschkinia* (Bacillariophyta) species and new insights into the genus phylogeny, European Journal of Phycology, 54:4, 609-631, DOI: [10.1080/09670262.2019.1628307](https://doi.org/10.1080/09670262.2019.1628307)

To link to this article: <https://doi.org/10.1080/09670262.2019.1628307>



[View supplementary material](#)



Published online: 27 Aug 2019.



[Submit your article to this journal](#)



Article views: 381



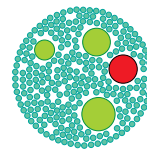
[View related articles](#)



[View Crossmark data](#)



Citing articles: 13 [View citing articles](#)



## Six new epibiotic *Proschkinia* (Bacillariophyta) species and new insights into the genus phylogeny

Roksana Majewska <sup>a,b</sup>, Sunčica Bosak <sup>b,c</sup>, Thomas A. Frankovich <sup>d</sup>, Matt P. Ashworth <sup>e</sup>, Michael J. Sullivan <sup>f</sup>, Nathan J. Robinson <sup>g</sup>, Eric A. Lazo-Wasem <sup>h</sup>, Theodora Pinou <sup>i</sup>, Ronel Nel <sup>j</sup>, Schonna R. Manning <sup>e</sup> and Bart Van de Vijver <sup>k,l</sup>

<sup>a</sup>Unit for Environmental Sciences and Management, School of Biological Sciences, North-West University, Potchefstroom, South Africa; <sup>b</sup>South African Institute for Aquatic Biodiversity (SAIAB), Grahamstown, South Africa; <sup>c</sup>Department of Biology, Faculty of Science, University of Zagreb, Zagreb, Croatia; <sup>d</sup>Florida Bay Interagency Science Center, Florida International University, Key Largo, Florida, USA; <sup>e</sup>Department of Molecular Biosciences, The University of Texas at Austin, Austin, Texas, USA; <sup>f</sup>130 Martinique Drive, Madison, MS 39110, USA; <sup>g</sup>Cape Eleuthera Institute, Cape Eleuthera Island School, Eleuthera, The Bahamas; <sup>h</sup>Division of Invertebrate Zoology, Peabody Museum of Natural History, Yale University, New Haven, Connecticut, USA; <sup>i</sup>Department of Biological and Environmental Sciences, Western Connecticut State University, Danbury, Connecticut, USA; <sup>j</sup>Department of Zoology, Institute for Coastal and Marine Research, Nelson Mandela University, Port Elizabeth, South Africa; <sup>k</sup>Research Department, Botanic Garden Meise, Meise, Belgium; <sup>l</sup>Department of Biology, University of Antwerp, ECOBE, Antwerpen, Belgium

### ABSTRACT

The diatom genus *Proschkinia* is a common element of biofilms covering diverse substrata in saline inland or shallow coastal environments. It can be distinguished from other naviculoid taxa by its lanceolate valves with a fistula located within the central area and numerous open girdle bands with a U-shaped cross-section and a single row of perforations on the internal side of the fold. Despite this distinct morphology, frustules of *Proschkinia* are typically weakly silicified and often overlooked when cleaned diatom material is analysed. The current paper describes six new species of *Proschkinia*: *P. browderiana* sp. nov., *P. lacrimula* sp. nov., *P. maluszekiana* sp. nov., *P. sulcata* sp. nov., *P. torquata* sp. nov. and *P. vergostriata* sp. nov., found in numerous samples of marine organisms, such as sea turtles (including sea turtle museum specimens), sea turtle-associated barnacles and seagrass from across the three oceans. Some of the newly described taxa were found on multiple individuals belonging to different sea turtle species, whereas others were in samples collected from different continents. Molecular phylogenetic analysis indicated that examined *Proschkinia* strains formed a monophyletic clade, sister to *Fistulifera*.

ARTICLE HISTORY Received 22 December 2018; Revised 18 April 2019; Accepted 3 May 2019

KEYWORDS Barnacle; epiphyte; epizoic; marine diatom; museum specimen; seagrass; sea turtle

### Introduction

Following the first reports focused on sea turtle-associated diatoms (Frankovich *et al.*, 2015; Majewska *et al.*, 2015a,b), the number of studies investigating microbial epibionts of sea turtles and new epizoic diatom species has grown steadily (Frankovich *et al.*, 2016; Robinson *et al.*, 2016; Majewska *et al.*, 2017a,b, 2018a,b; Riaux-Gobin *et al.*, 2017a,b; Kaleli *et al.*, 2018; Rivera *et al.*, 2018). Several diatom species belonging to known or new genera have been described in the last four years (Frankovich *et al.*, 2015, 2016; Majewska *et al.*, 2015a, 2017a, 2018a,b; Riaux-Gobin *et al.*, 2017a,b; Kaleli *et al.*, 2018). It has been suggested that a better understanding of sea turtle diatoms may complement our knowledge on the ecology of the host animal, providing additional information on individual sea turtle migration routes, location of its feeding pastures, in-water behaviour and overall well-being, as compositional changes in the diatom community would be linked directly to the external (e.g. environmental changes caused by changing

latitude or distance from the coast) and internal (e.g. disease, injuries, ageing) factors affecting the host (Robinson *et al.*, 2016). Should this hypothesis prove correct, diatom-based indices of, for example, sea turtle health or swimming patterns may be developed in the future. However, detailed data on still poorly known diatom communities growing on sea turtles worldwide must be gathered prior to making such inferences. Currently, it is still unclear to what degree the sea turtle diatom communities overlap with those encountered by the animals within their feeding, grooming or mating areas. While some diatom taxa seem to be well-adapted to the challenging conditions on the animal body surface and may constitute a key element of the pioneer epizoic communities, some other species may be able to attach to and thrive on the sea turtle skin or carapace only at the later stages of biofilm formation (Majewska *et al.*, 2017b, 2018a).

The diatom genus *Proschkinia* was erected in 1978 by Karayeva to accommodate three morphologically distinct

marine naviculoid taxa, *P. bulnheimii* (Grunow) Karayeva, *P. tubulifera* (Geissler & Gerloff) Karayeva and *P. complanatoides* (Hustedt) Karayeva (Karayeva, 1978). Although *Proschkinia* species clearly differ from other members of *Navicula sensu lato* in having, for instance, a fistula internally occluded by domed hymen(es) within the central area and numerous folded girdle bands (resulting in a long pervalvar axis) with a single row of perforations on the internal side of the fold, they are often overlooked or probably misidentified during a routine diatom analysis due to weakly silicified and fragile frustules (Underwood & Yallop, 1994). Other features typical of *Proschkinia* include two girdle-appressed, lobed and offset (towards opposite poles) chloroplasts, lanceolate valves, fine, almost parallel striae becoming convergent close to the apices, a prominent raphe-sternum and an asymmetrical central area (Karayeva, 1978; Cox, 1981, 2012; Brogan & Rosowski, 1988). Currently, there are seven species known to belong to the genus, all of which are found in either marine or saline inland habitats (Cholnoky, 1963; Ehrlich, 1978; Lange & Tiffany, 2002; Lobban *et al.*, 2012; Pichierri *et al.*, 2017). Despite *Proschkinia* being highly motile, it is found in both surface-associated biofilms and planktonic communities (Riznyk, 1973; Hillebrand & Sommer, 2000; Lange & Tiffany, 2002; Barinova & Krupa, 2017; Pezzolesi *et al.*, 2017).

Only very recently have the first molecular data on *Proschkinia* been provided. Gastineau *et al.* (2019) sequenced the complete mitochondrial genome of one *Proschkinia* strain and compared the obtained results with available information on mitochondrial genes of other diatom taxa. According to the maximum-likelihood phylogenetic analysis performed, the examined strain of *Proschkinia* sp. was sister to *Fistulifera solaris*, thus confirming the previous hypotheses of other authors, who noticed the intriguing similarity in fistula structure between the two genera (Cox, 2012; Zgrundo *et al.*, 2013). However, this analysis was limited to a dataset which comprised only 14 raphid diatoms out of thousands of described species, including additional taxa with fistula-like structures.

The current paper describes six new *Proschkinia* species growing on living marine substrata, such as sea turtles (including six sea turtle species), sea turtle-associated barnacles (*Chelonibia testudinaria* Linnaeus and *Platylepas coriacea*), and seagrass (*Thalassia testudinum*) from various geographic localities. The new taxa, *P. browderiana* Frankovich, Ashworth & Sullivan, sp. nov., *P. lacrimula* Majewska, sp. nov., *P. maluszekiana* Majewska, sp. nov., *P. sulcata* Majewska, Van de Vijver & Bosak, sp. nov., *P. torquata* Bosak, Van de Vijver & Majewska, sp. nov. and *P. vergostriata* Frankovich, Ashworth & Sullivan, sp. nov., were found during numerous surveys carried out over a span of four years, during which a large number of hosts and samples

(including sea turtle museum specimens) were investigated. Furthermore, this study offers new insights into the phylogeny of the genus *Proschkinia* based on a 3-gene phylogenetic analysis of several *Proschkinia* strains, including several isolated from sea turtles, and related diatom taxa.

## Materials and methods

### Material collection and microscopy

Diatom samples were collected from various biotic habitats located within three different ocean basins using either a toothbrush, a cotton-tipped applicator, a razor blade or sonication to detach diatoms from their substratum (Table 1, Fig. 1). Standard cleaning methods were applied to remove the organic matter and enable microscopic analyses of diatom frustules (Table 1). Altogether more than 100 samples and 200 *Proschkinia* specimens were analysed. The morphologies of the new taxa have been compared with descriptions and images of all known *Proschkinia* species (Brockmann, 1950; Cholnoky, 1963; Karayeva, 1978; Archibald, 1983; Simonsen, 1987; Brogan & Rosowski, 1988; Cox, 1988, 1998, 2012; Round *et al.*, 1990; Witkowski *et al.*, 2000; Clavero i Oms, 2009; Karayeva & Bukthiyarova, 2010; Zgrundo *et al.*, 2013). The taxonomic terminology used in the current paper largely follows Hendey (1964), Ross & Sims (1972), Anonymous (1975), Ross *et al.* (1979), Round *et al.* (1990) and Cox (2012).

### Culturing

Cells were isolated from collected samples by glass micropipette into 16 × 100 mm glass culture tubes filled with 34 psu f/2 growth medium (Guillard, 1975). Strains related to this manuscript were maintained on a laboratory bench lit by natural light from a north-facing window, at a temperature of 20–24°C. Once isolate growth was recorded, the culture was split into two parts: one for microscopy and one for DNA extraction. The microscopy split was cleaned with a 1:1:1 mix of culture medium, 30% hydrogen peroxide and 70% nitric acid, and then washed with distilled water until the pH was neutral. Cleaned cultured material was dried onto 22 × 22 mm glass coverslips for light microscopy (LM) and 12 mm diameter glass coverslips for scanning electron microscopy (SEM). Permanent slides of cultured material were mounted with Naphrax mounting medium (Brunel Microscopes, [www.brunelmicroscopessecure.co.uk](http://www.brunelmicroscopessecure.co.uk)). Coverslips for SEM observation were mounted onto aluminium stubs and coated with iridium using a Cressington 208 Bench Top Sputter Coater (Cressington Scientific Instruments, Watford, UK) and observed with a Zeiss SUPRA 40 VP scanning electron microscope (Carl Zeiss Microscopy, Thornwood, New York, USA).

**Table 1.** Material collection and treatment methods and equipment used in the current study.

Collection date	Collection site	Substratum	Collection method/ tool	Cleaning procedure	LM observations	SEM microscope	Sputter-coater/ material	Culture
<i>P. bryoderiana</i> 28 March 2016	Biscayne Bay, FL, USA	seagrass <i>Thalassia testudinum</i> blades	razor blade	digestion in boiling 30% $\text{HNO}_3$ with addition of $\text{K}_2\text{Cr}_2\text{O}_7^{\text{a}}$	Nikon E600 microscope with DIC*, Leica DFC425 digital camera	Zeiss SUPRA 40 VP	Cressington 208 Bench Top Sputter Coater/iridium	No
<i>P. lacrimula</i> 20 December 2012 29 July 2014	Riverhead, NY, USA	Kemp's ridley carapace Kemp's ridley carapace green turtle carapace	sonication <sup>b</sup>	rapid digestion in boiling 64% $\text{HNO}_3$ and 97% $\text{H}_2\text{SO}_4^{\text{c}}$	Nikon 80i light microscope with DIC*, Nikon DS-Fi1 5MP digital camera	FEI Quanta Feg 250	Cressington 108Auto/ gold-palladium	No
<i>P. maluszekiana</i> 20 December 2012 29 July 2014 15–20 December 2017	Riverhead, NY, USA Kosi Bay, KwaZulu Natal, South Africa	Kemp's ridley carapace green turtle carapace loggerhead carapace sea turtle associated barnacles <i>Chelonia testudinaria</i>	sonication <sup>b</sup> toothbrush razor blade (to detach barnacles) and sonication <sup>b</sup>	rapid digestion in boiling 64% $\text{HNO}_3$ and 97% $\text{H}_2\text{SO}_4^{\text{c}}$	Nikon 80i light microscope with DIC*, Nikon DS-Fi1 5MP digital camera	FEI Quanta Feg 250	Cressington 108Auto/ gold-palladium	No
<i>P. sulcata</i> 6–12 October 2013 unknown (Robinson et al., 2016)	Ostional, Costa Rica Hawaii, USA Florida, USA South Carolina, USA	olive ridley carapace hawksbill carapace loggerhead carapace	razor blade sonication <sup>b</sup>	rapid digestion in boiling 64% $\text{HNO}_3$ and 97% $\text{H}_2\text{SO}_4^{\text{c}}$	Nikon 80i light microscope with DIC*, Nikon DS-Fi1 5MP digital camera	FEI Quanta Feg 250	Cressington 108Auto/ gold-palladium	No
November 2015– February 2016; December 2017– February 2018 December 2017– February 2018 30 September 2016 18–20 October 2018	Kosi Bay, KwaZulu Natal, South Africa Marine Turtle Rescue Centre, Pula, Croatia	sea turtle associated barnacles <i>Chelonia testudinaria</i> and <i>Platylepas coriacea</i> loggerhead carapace and skin and leatherback skin loggerhead carapace	razor blade (to detach barnacles) and sonication <sup>b</sup> toothbrush razor blade, toothbrush	heated 37% $\text{H}_2\text{O}_2$ with addition of $\text{KMnO}_4^{\text{d}}$	Zeiss Axioimager A2 with DIC*, Axiocam 305 digital camera	Zeiss Ultra Plus	Cressington 208HR	TB0019**
<i>P. torquata</i> November 2015– February 2016; December 2017– February 2018 December 2017– February 2018 30 September 2016	Kosi Bay, KwaZulu Natal, South Africa Marine Turtle Rescue Centre, Pula, Croatia	sea turtle associated barnacles <i>Chelonia testudinaria</i> loggerhead carapace	razor blade (to detach barnacles) and sonication <sup>b</sup> toothbrush razor blade	rapid digestion in boiling 64% $\text{HNO}_3$ and 97% $\text{H}_2\text{SO}_4^{\text{c}}$	Nikon 80i light microscope with DIC*, Nikon DS-Fi1 5MP digital camera	FEI Quanta Feg 250	Cressington 108Auto/ gold-palladium	No
<i>P. vergastriata</i> 24 June–1 July 2015 24 May 2016 22 March 2017	Florida Bay, FL, USA Turtle Hospital, Marathon, FL, USA	loggerhead skin (neck) green turtle skin (neck and flipper) loggerhead skin (neck and flipper)	cotton-tipped applicator toothbrush	digestion in boiling 30% $\text{HNO}_3$ with addition of $\text{K}_2\text{Cr}_2\text{O}_7^{\text{a}}$	Nikon E600 microscope with DIC, Leica DFC425 digital camera	Zeiss SUPRA 40 VP	Cressington 208 Bench Top Sputter Coater/ iridium	HK551, 552*** HK548, HK549, HK500*** No

References: <sup>a</sup>Frankovich et al., 2018; <sup>b</sup>Majewska et al., 2018; <sup>c</sup>Hasle & Syvertsen 1997; <sup>d</sup>van der Werff 1955. \*Differential Interference Contrast; \*\*see Supplementary fig. S1; \*\*\*see Supplementary figs S1–S3.

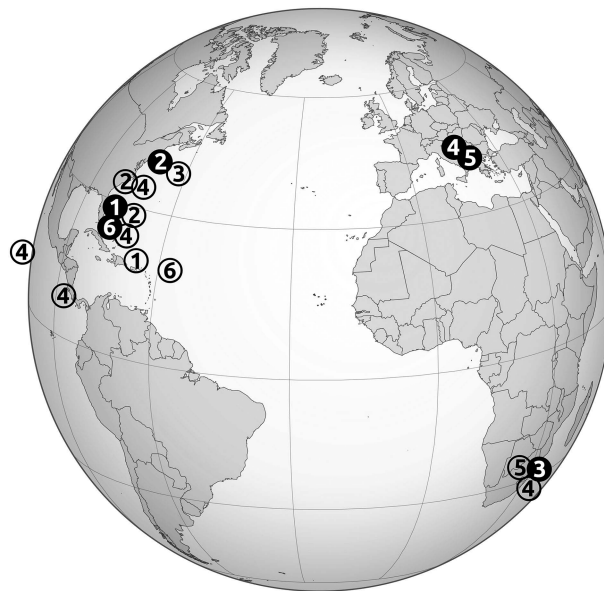


**Fig. 1.** Locations of the six *Proschkinia* species. Solid black circles indicate type locations. 1 – *P. browderiana*, 2 – *P. lacrimula*, 3 – *P. maluszekiana*, 4 – *P. sulcata*, 5 – *P. torquata*, 6 – *P. vergostriata*.

Strain TB0019 (*P. sulcata* sp. nov.) was isolated from the sample obtained from loggerhead turtle skin on 20 October 2018 (Table 1). The single cell was isolated in a similar manner as described above, placed into a sterile 60 × 15 mm plastic Petri dish filled with 38 psu f/2 medium. The culture was maintained in a plastic culture flask with 30 ml of f/2 medium under constant temperature of 20–22°C and photoperiod of 12 h of light. The material for morphological analyses was cleaned and prepared for LM and SEM observations as described in Mejdandžić *et al.* (2018). The samples were sputter coated with ~10 nm layer of gold using the Precision Etching and Coating System, PECS II (Gatan Inc., California, USA) and observed using a JSM-7800F scanning electron microscope (JEOL Ltd., Tokyo, Japan).

#### DNA preparation and phylogenetic analysis

Cultured material for DNA extraction was centrifuged in a Sorvall ST 16R benchtop centrifuge (Thermo Electron, Germany) for 20 min at 5000 rpm. Pellets were extracted with a QIAGEN DNeasy Plant Mini Kit (QIAGEN Sciences, Valencia, California, USA), using 1.0 mm glass beads in a Mini-Beadbeater (Biospec Products, Inc, Bartlesville, Oklahoma, USA) for 45 s for cell disruption and frustule breakage. Polymerase chain reaction (PCR) amplification and sequencing of small-subunit nuclear rRNA and the chloroplast-encoded *rbcL* and *psbC* markers followed the primers and protocols of Theriot *et al.* (2015) and Li *et al.* (2016). Extracted DNA and culture material not currently in public collections, as well as DNA extraction photovouchers, are available upon request from MPA at University of Texas - Austin. A list

of isolates and corresponding GenBank accession numbers is provided in Supplementary table S1.

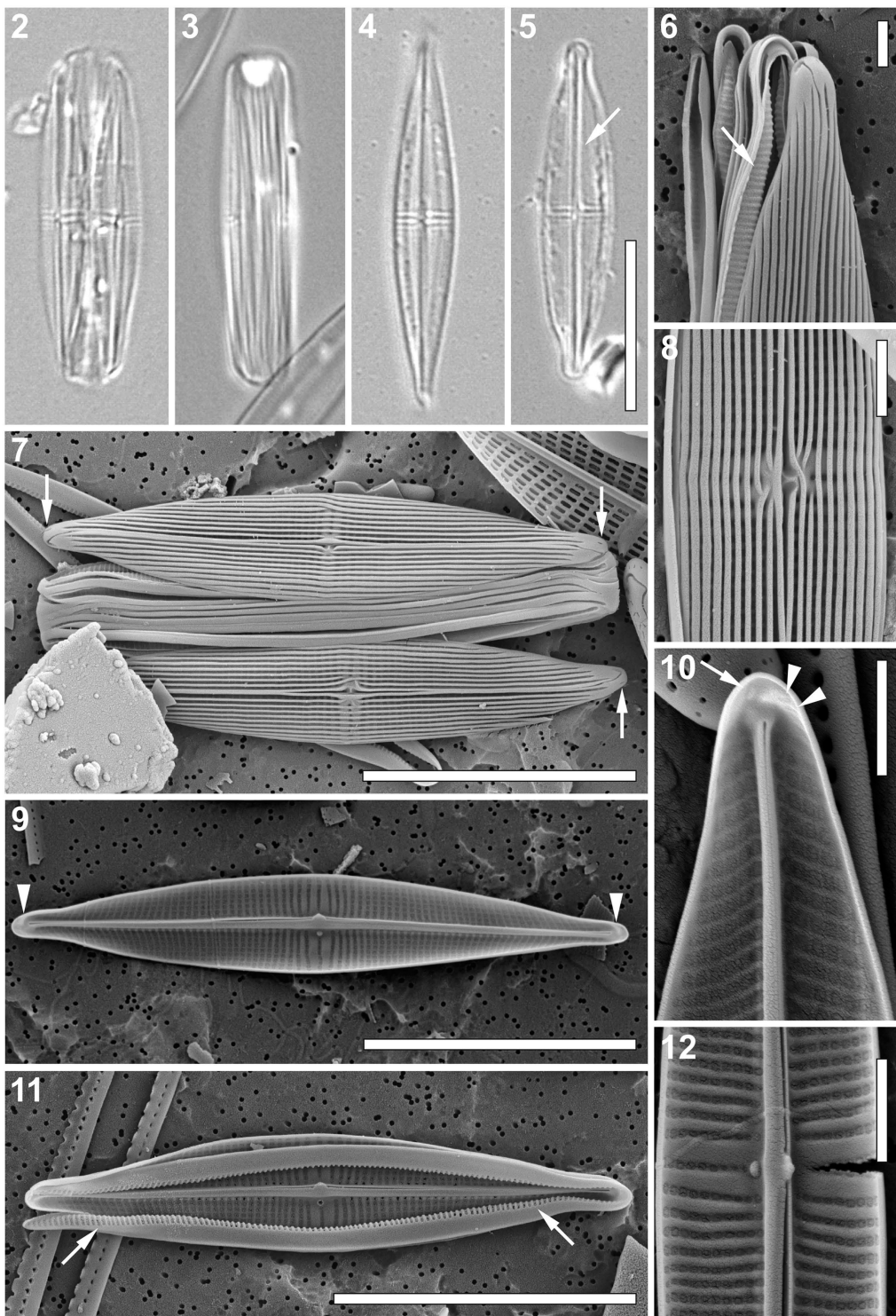
#### Phylogenetic analyses

Sequences generated for this manuscript were added to a concatenated dataset of sequences from three genes (SSU, *rbcL* and *psbC*) presented in Sabir *et al.* (2018). Sequence data from two *Asterionellopsis socialis* and one *Asterionellopsis glacialis* strains were used as outgroups. The secondary structure of the nuclear ribosomal SSU sequences was aligned by SSU-align (Nawrocki, 2009) by covariance models; ambiguous sites with a posterior probability less than the default of 0.9 were removed. Aligned datasets are available in Supplementary data S1. The dataset was partitioned by marker, by codon position for *rbcL* and *psbC* and by paired vs unpaired sites for SSU. A maximum likelihood (ML) analysis was performed using RAxML v8.1 (Stamatakis, 2014), under a GTR + G + I model, with the best tree chosen from 30 runs using the rapid bootstrap analysis with 1000 bootstrap replicates. The dataset was also analysed under maximum parsimony (MP) using TNT (Goloboff *et al.*, 2008) by the ‘New Technology Search’ option with ‘Sectorial Search’ and ‘Tree Fusing’ set to default parameters. Ratchet and Drift were set to default settings, except that the total number of iterations (‘ratchet’) or cycles (‘drift’) of each was set to 100. Three runs with 25 random addition sequences each were made and recovered tree files from each run were concatenated in Winclada (Nixon, 2002), where a strict consensus tree was calculated. For bootstrap analysis, search conditions were re-set to Sectorial Search, Ratchet, Drift, Tree Fusing all at default settings, with 10 random additions each. Bootstrapping was set to ‘sample with replacement’ with 1000 BS replicates.

#### Results

##### *Proschkinia browderiana* Frankovich, Ashworth & M.J. Sullivan, sp. nov. (Figs 2–12)

**Light microscopy (Figs 2–5):** Frustules usually observed with partially detached valves lying in valve view (Fig. 2), fully intact frustules (Fig. 3) rarely seen. Frustules weakly silicified, 4–6 µm wide ( $n = 6$ , natural population), rectangular in girdle view showing rounded apices and numerous narrow copulae (Figs 2, 3). Valves lanceolate with rounded, protracted (Fig. 4) to rostrate apices (Fig. 5). Valve dimensions ( $n = 30$ ): length 18.0–31.5 µm, width 3–4 µm, length to width ratio 4.8–7.8. Axial area very narrow with distinct sternum (Fig. 5, arrow).



**Figs 2–12.** *Proschnia browderiana* sp. nov. **Figs 2–5.** Light micrographs. **Fig. 2.** Specimen with partially detached valves. **Fig. 3.** Girdle view. **Figs 4, 5.** Valve view. Arrow indicates a distinct sternum. **Figs 6–12.** Scanning electron micrographs. **Fig. 6.** Apical part of the frustule, showing multiple girdle bands with transapically elongated pores forming a comb-like appearance (arrow). **Fig. 7.** Specimen with partially detached valves. Arrows indicate apically elongated slits present at the valve apices on the primary side of the valve. **Fig. 8.** Central part of the valve (external view). **Fig. 9.** Internal view of the valve with curved thickenings at the apices (arrowheads). **Fig. 10.** Internal view of the apical part of the valve with a single areola present on the primary side of the valve (arrow) and two small areolae at the end of the hooked thickening (arrowheads). **Fig. 11.** Internal view of the valve with a partially detached valvocopula. Arrows indicate the transapically elongated pores on the internal side of the girdle band. **Fig. 12.** Central part of the valve (internal view). Scale bars: Figs 2–5, 7, 9, 11: 10 µm, Figs 6, 8, 10, 12: 1 µm.

Central area barely distinguishable, showing 2–4 more distantly spaced central striae on both sides of raphe. Other striae indiscernible in LM (Figs 2–5).

*Scanning electron microscopy* (Figs 6–12). *External view:* Valve face covered by relatively narrow longitudinal cord-like silica strips running nearly continuously from apex to apex with only small breaks and deflections around the central area, lying noticeably above the plane of the striae (Figs 6–8). Near the apices, silica strips fused to form a small pore-free area (Figs 6, 7). Areolae weakly visible in the grooves formed between the longitudinal strips (Figs 6–8). Virgae noticeably wider in the valve middle (Fig. 8). Mantle shallow, lacking a clear transition between valve face and mantle (Fig. 7). A single apically elongated slit present at the valve apices on the primary side of the valve (Fig. 7, arrows). Raphe straight, located between two thickened longitudinal strips. Strips opening near the central raphe endings (Fig. 7). Central raphe endings very closely spaced, slightly bent towards the secondary side of the valve, spathulate with raised silica rims (Fig. 8). Terminal raphe fissures strongly hooked towards the secondary side, extending onto the valve mantle (Figs 6, 7). Fistula opening not evident, obscured by a pocket-like silica flap formed by two fused thickened longitudinal strips on the primary side of the valve (Fig. 8).

*Internal view:* Uniseriate striae nearly parallel to very slightly radiate in the valve middle becoming slightly curved and finally convergent near the apices (Figs 9–12), 38–43 in 10 µm. Striae separated by clearly raised virgae (Fig. 12), composed of rectangular to almost square areolae, occluded by hymenes (Figs 9–12), ca. 60 in 10 µm. Raphe branches visible only near the central area and at the apices, opening laterally on the secondary side of the valve within a thick axial rib (Figs 9–12). Central raphe endings straight, simple (Figs 9, 10). A wafer-like silica thickening with a small blunt tip on the central nodule extending laterally towards the secondary side of the valve from the axial rib (Figs 9, 11, 12). Fistula opening covered by a nearly circular domed structure, located at the end of a shortened central stria close to the axial area, not reaching the axial rib (Figs 9, 11, 12). Terminal raphe endings elongated, lying laterally on the sternum, terminating onto simple helictoglossae. Small pore-free area present at the apices. Apices showing a slight thickening corresponding to the hooked terminal raphe fissure on the external surface of the valve with up to two small areolae at the end of the thickening (Figs 9, 10, arrowheads). Single areola present at the apices on the primary side of the valve (Fig. 10, arrow).

Cingulum composed of multiple open copulae (Figs 6, 7, 11), folded with the fold on the cell interior showing a row of hymenate, transapically elongated pores forming a comb-like appearance (Figs 6, 11, arrows); pore density ca. 7 in 1 µm. Pars exterior plain (Figs 6, 7, 11).

*Taxonomic remarks:* *P. browderiana* is most similar to *P. bulnheimii*, sharing rounded protracted apices and longitudinal cord-like silica strips on the valve face. *P. browderiana* can be distinguished from *P. bulnheimii* by its higher stria density (38–43 in 10 µm versus ca. 22 in 10 µm) and a different valve outline. *P. browderiana* has a lanceolate valve outline whereas *P. bulnheimii* presents a linear lanceolate valve outline. The stria pattern also differs between the species, being nearly parallel in the valve middle becoming convergent near the apices in *P. browderiana* but nearly parallel throughout in *P. bulnheimii*. Furthermore, the external cord-like longitudinal silica strips continue on the valve face of *P. browderiana* but are interrupted over the widened virgae in *P. bulnheimii*. The internal opening of the fistula is located at a short distance from the central nodule and axial rib in *P. browderiana* but in *P. bulnheimii* the opening is located at the junction of the axial rib and the internal valve face. Clavero i Oms (2009) presents both LM (fig. 82: 1–8) and SEM (fig. 82: 9–26) images of *Proschkinia* specimens belonging to several populations from different geographic regions. Although the author tentatively identified specimens collected in Spain (fig. 82: 1–3, 9, 12–14, 19, 23, 24) and Mexico (fig. 82: 4–8, 10, 11, 15–18, 20–22, 25, 26) as *P. bulnheimii*, only the former exhibit features that agree with the original protologue. Specimens collected in Mexico (Guerrero Negro, Baja California) resemble *P. browderiana* in having a clearly lanceolate valve outline (fig. 82: 4 and 5 in Clavero i Oms, 2009), a high stria density (up to 45 in 10 µm) and an internal fistula opening located close to the axial area, but not on the junction of the axial rib and the valve face surface (fig. 82: 25 in Clavero i Oms, 2009).

**HOLOTYPE:** Permanent slide BR-4558 and unmounted material deposited in the BR-collection housed by Botanic Garden Meise, Belgium.

**ISOTYPES:** Permanent slide SANDC-ST001 deposited in the South African Diatom Collection housed by North-West University, Potchefstroom, South Africa and permanent slide DH 311958 and unmounted material DH 311959 deposited in the Academy of Natural Sciences of Drexel University, Philadelphia, Pennsylvania, USA.

**TYPE LOCALITY:** Biscayne Bay, Florida, USA (25°30'16" N, 80°20'16"W). Collected from the leaves of the seagrass *Thalassia testudinum* by A. Wachnicka, 28 March 2016.

**ETYMOLOGY:** The epithet honours Dr Joan Browder (United States National Oceanic and Atmospheric Administration, Miami, Florida) in recognition of her decades of research on the ecology of Biscayne Bay.

**ECOLOGY:** Epiphytic on the seagrass *T. testudinum* in Biscayne Bay, Florida (USA).

***Proschkinia lacrimula* Majewska, sp. nov. (Figs 13–22)**

**Light microscopy (Figs 13–14):** Intact frustules not observed. Frustules very weakly silicified and very fragile (Figs 13, 14). Valves narrow, linear-lanceolate to lanceolate, with bluntly rounded, slightly rostrate apices, often broken along the raphe, with chipped edges, and folded (Figs 13, 14). Valve dimensions ( $n = 30$ ): length 6–13 µm, width 1.5–3 µm, length/width ratio 3.5–6.1. Striae and raphe structure indiscernible in LM. Slightly off-centre fistula visible as glistening dot in the central area (Fig. 14). Girdle bands open, appearing unornamented (Figs 13, 14).

**Scanning electron microscopy (Figs 15–22). External view:** Valve face flat showing smooth surface lacking longitudinal silica strips, with a gradually curving valve face/mantle junction and shallow mantle (Figs 15–18). Striae uniserial, parallel throughout almost the entire valve, becoming very slightly convergent towards the apices, comprised of a single row of apically elongated lineate areolae, perpendicular to the sternum (Figs 15–18). Longitudinal row of areolae bordering the axial area apparently sunken and partially covered by a very narrow conopeum extending from the axial ridge bordering the raphe branches (Figs 15–18). Axial area very narrow, formed by a slightly raised raphe-sternum composed of two raised silica strips (Figs 15–18). Raphe branches almost straight to very slightly curved, with slightly expanded, pore-like central endings deflected towards the fistula (Figs 15, 17, 18). Central area asymmetrical due to a shortened central stria present on the secondary valve side and the rounded fistula opening on the opposite side of the raphe-sternum (primary side; Figs 15, 17, 18). Terminal raphe fissures strongly hooked towards the secondary side of the valve (Figs 15–17). Several irregular hymenate areolae embedded within terminal fissure (Fig. 16, arrowheads). A single row of sparse elongated or irregular areolae near valve apex on primary side of the valve (Figs 15–17, arrows).

**Internal view:** Striae extending from the very narrow pore-free margin to the prominent axial rib (Figs 19–21), 38–45 in 10 µm ( $n = 30$ ), composed of squarish to rectangular uniformly sized areolae, occluded by

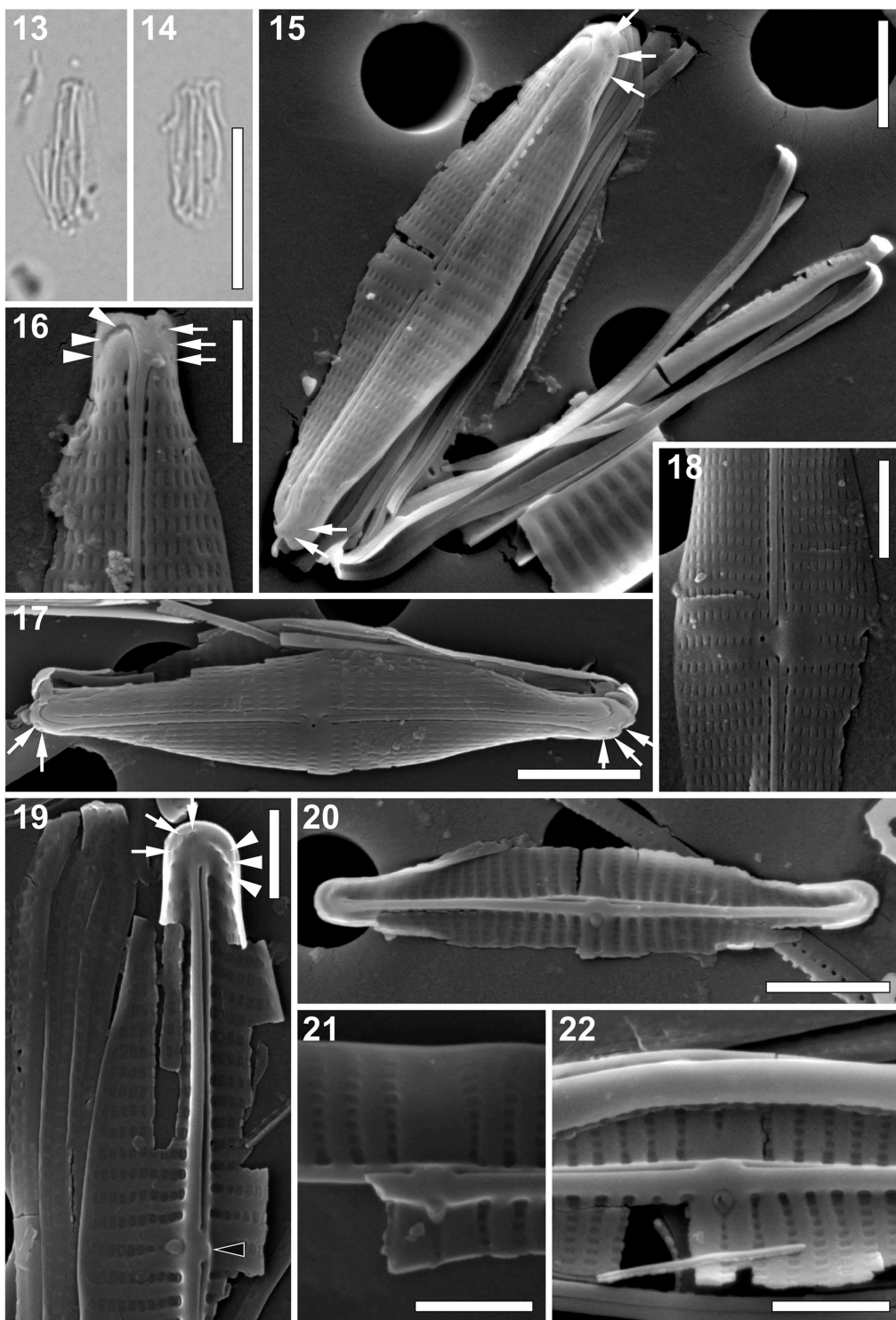
hymenes (Figs 19–21). Central areolae roundish, clearly raised on the axial rib, perpendicular to the valve face surface (Figs 19–21). Fistula opening occluded by a teardrop-shaped, domed hymen, located on the primary side of the raphe-sternum (Figs 19–21). Raphe slit opening laterally on the raphe-sternum, to the secondary side of the valve and opposite to the fistula (Figs 19–21). Central raphe endings very slightly expanded, slightly deflected towards the fistula (Figs 19, 21). A small, ridge-like, rounded and oblate lateral thickening present on the central rib, between the central raphe endings (Fig. 19, black arrowhead). Terminal raphe endings slightly twisted, terminating onto weakly developed helictoglossae, merging with slightly hooked thickenings corresponding to the terminal raphe fissures on the external surface of the valve (Figs 19, 21). Areolae at the end of the thickenings (up to three; Fig. 19, arrows) and those at the apices occluded by hymenes (up to four; Fig. 19, arrowheads).

**Cingulum** composed of multiple open copulae (Figs 15, 19). Pars interior showing a row of hymenate, squarish pores (Fig. 19), ca. 6 in 1 µm. Pars exterior plain (Fig. 15).

**Taxonomic remarks:** The high number of broken valves may be related to the fact that these specimens were extracted from sea turtle museum specimens using sonication – a method that may potentially contribute to the breaking of weakly silicified frustules (R. Majewska, pers. obs.). Moreover, it is not clear whether and how the preservation methods and handling procedures applied at the museum affected the epizoic diatom frustules still present on the animal surface.

This taxon can be easily confused with weakly silicified specimens of *Poulinea* and *Chelonicola* dominating every sample in which *P. lacrimula* was observed. In addition, the less frequent and less abundant *Labellicula lecohuiana* was present in some of these samples. All mentioned taxa are similar in size to *P. lacrimula*, possess almost undiscernible striae (especially in smaller specimens), and numerous, sometimes partially detached and broken girdle bands that may resemble those of *P. lacrimula*. In both *Poulinea* and *Chelonicola* the central raphe endings may appear as a single glistening dot resembling a fistula. *P. lacrimula* can usually be discriminated from *Poulinea* and *Chelonicola* by its slightly rostrate apices, although these may be indistinct in broken or folded valves, whereas *L. lecohuiana* possesses both rostrate apices and an isolated pore (Majewska *et al.*, 2018b).

*P. lacrimula*, although similar in size to *P. vergostriata*, can be distinguished from the latter by differences in valve



**Figs 13–22.** *Proschkinia lacrimula*. **Figs 13, 14.** Light micrographs showing damaged specimens. **Figs 15–22.** Scanning electron micrographs. **Fig. 15.** Specimen with partially detached girdle bands. Arrows indicate elongated areolae present at the valve apices. **Fig. 16.** Apical part of the valve, showing three irregular hymenate areolae embedded within terminal fissure (arrowheads) and a single row of elongated areolae on primary side of the valve close to the valve margin (arrows). **Fig. 17.** External view of the valve. Arrows indicate the elongated areolae on primary side of the valve at the apices. **Fig. 18.** Central part of the valve (external view). **Fig. 19.** Internal view of the apical part of the valve with a single row of areolae present on the primary side of the valve (arrows) and three small areolae at the end of the hooked thickening (arrowheads). **Fig. 20.** Internal view of the valve. **Fig. 21.** Central part of the valve (internal view). **Fig. 22.** Internal view of the central part of the valve with missing occlusion of the fistula. Scale bars: Figs 13, 14: 10 µm, Figs 15, 17, 20: 2 µm, Figs 16, 18–22: 1 µm.

outline, stria structure, areola shape and fistula morphology (Table 2). Both taxa occur epizooically on sea turtles from the north-western Atlantic Ocean and are the only species of the genus completely lacking longitudinal silica strips on the valve face. However, *P. lacrimula* has slightly rostrate apices, nearly parallel striae becoming only slightly convergent at the apices, and apically elongated, linear areolae. Externally, the fistula opening is a simple unobscured pore, whereas the internal teardrop-shaped occlusion lies laterally on the uniformly thick central part of the axial rib. In contrast, *P. vergostriata* has rounded rather than rostrate apices, strongly curved and divergent striae, and broadly rectangular areolae. The external fistula opening is obscured by a linear silica flange. Internally, the oval fistula occlusion lies on lateral expansion of the central nodule (Table 2).

**HOLOTYPE:** Permanent slide BR-4459 and unmounted material deposited in the BR-collection housed by Botanic Garden Meise, Belgium.

**ISOTYPES:** Permanent slide SANDC-ST002 and unmounted material (sample TPD-05) deposited in the South African Diatom Collection housed by North-West University, Potchefstroom, South Africa, and permanent slide TPD05-16 deposited at the Yale Peabody Museum of Natural History, New Haven, USA.

**PARATYPES:** Permanent slides SANDC-TPD06-18 and SANDC-TPD21-18 and unmounted material (samples TPD-06 and TPD-21) deposited in the South African Diatom Collection housed by North-West University, Potchefstroom, South Africa.

**TYPE LOCALITY:** Riverhead, New York, USA. Taken from the carapace of:

- (1) a juvenile Kemp's ridley (*Lepidochelys kempii*) found cold-stunned (and beyond rehabilitation) on the beach by an anonymous collector, 20 December 2012 (holotype and isotypes);
- (2) a juvenile Kemp's ridley (*L. kempii*) found cold-stunned (and beyond rehabilitation) on the beach by an anonymous collector, 29 July 2014 (paratype);
- (3) a juvenile green turtle (*Chelonia mydas*) found cold-stunned (and beyond rehabilitation) on the beach by an anonymous collector, 29 July 2014 (paratype).

**ETYMOLOGY:** From the Latin word *lacrimula* ('little tear') with reference to the teardrop-shaped occlusion of the fistula.

**ECOLOGY:** Epizoic on juvenile Kemp's ridleys *L. kempii*, loggerheads *Caretta caretta* and green turtles *C. mydas* from Long Island (New York, USA), an adult loggerhead found in the same location, and on adult

loggerheads from the eastern coasts of Florida and South Carolina (USA).

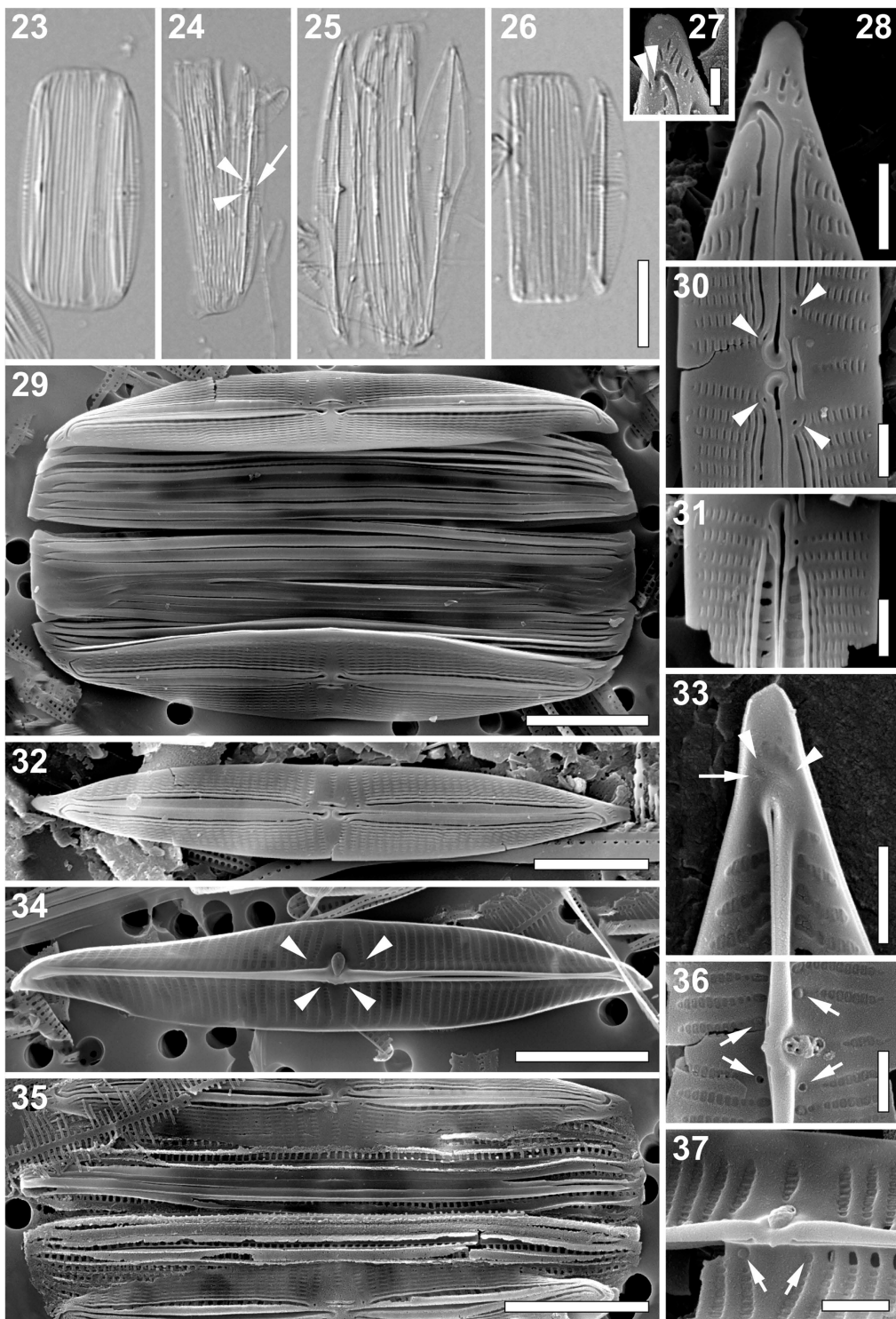
***Proschkinia maluszekiana* Majewska, sp. nov.**  
(Figs 23–37)

**Light microscopy (Figs 23–26):** Frustules in girdle view broad with numerous girdle bands (Figs 23–26). Valves weakly silicified and fragile, lanceolate with clearly convex margins and not protracted, cuneately rounded apices (Figs 24–26). Valve dimensions ( $n = 30$ ): length 22–36  $\mu\text{m}$ , width 3.5–5  $\mu\text{m}$ , length/width ratio 5.6–7.1. Raphe-sternum prominent (Figs 24–26). Central raphe endings rimmed (Fig. 24, arrowheads). Striae very fine, barely discernible throughout most of the valve but clearly visible, much sparser and strongly convergent near the central area (Figs 23–26), 26–30 in 10  $\mu\text{m}$ . Both the transapically elongated fistula occlusion (Fig. 25) and the apically elongated thickenings flanking the fistula opening (Fig. 24, arrow) clearly visible on one side of the raphe-sternum. Areolae adjacent to the sternum clearly larger, lying in a slightly different focal plane than the rest of the valve (Fig. 26). Girdle bands open, appearing unornamented (Figs 23–26).

**Scanning electron microscopy (Figs 27–37).** *External view:* Valve face flat. Near the axial area, several (up to 3 on each side of the raphe) longitudinal silica strips running from apex to the central area (Figs 28–32). Mantle very shallow, valve margins straight (Figs 29, 32). Striae uniserial, opposite and slightly convergent throughout almost the entire valve, becoming strongly convergent close to the apices and alternating with one another near the central area. Striae composed of lineate, apically elongated areolae (Figs 28–32). Longitudinal rows of areolae closest to the raphe clearly larger, rectangular, transapically elongated, usually entirely covered by a relatively broad conopeum (Figs 28–32, 35). Fistula transapically elongated, partially hidden by two silica flanges present on the primary side of the central area (Figs 29–32). Raphe branches straight to weakly curved with elongated, simple central endings, slightly deflected towards the isolated pore, flanked by distinct teardrop-shaped silica rims, giving the impression of central endings being expanded and deflected away from the fistula (Figs 29–32). Central area strongly asymmetrical due to a shortened central stria present next to the fistula on one side of the raphe (Figs 29–32). Four rounded pores adjacent to each of the striae bordering the central area present, partially hidden under the silica flanges on the secondary side (Fig. 30, arrowheads). Terminal raphe fissures strongly hooked towards the secondary side of the valve (Figs 27–29, 32), sometimes

**Table 2.** Main characters of the six new *Prosckinia* species.

Character	<i>P. browderiana</i>	<i>P. lacrimula</i>	<i>P. maluszekiana</i>	<i>P. sulcata</i>	<i>P. torquata</i>	<i>P. vergostriata</i>
Valve outline	lanceolate with rounded, protracted to rostrate apices	linear-lanceolate to lanceolate, with bluntly rounded, slightly rostrate apices	lanceolate, with cuneately rounded apices	narrowly lanceolate with elongated acutely rounded to very slightly rostrate apices	narrowly lanceolate with slightly protracted, cuneately rounded apices	narrowly lanceolate with weakly protracted, substrate to cuneately rounded apices
Valve length (μm)	18–31.5	6–13	22–36	10–28	21–32	5–15
Valve breadth (μm)	3–4	1.5–3	3.5–5	2.5–4	3–5	1.5–3
Length to width ratio	4.8–7.8	3.5–6.1	5.6–7.1	4.0–7.4	5.6–7.9	3.9–6.2
Stria density (in 10 μm)	38–43	38–45	26–30	40–45	28–32	27 (central area)–43 (apex)
Longitudinal silica strips	cord-like, covering entire valve face	absent	up to 3 on each side of the raphe	cord-like, covering almost entire valve face	interrupted at the central area, flattening near the valve margins	absent
Conopeum	absent	very narrow simple pore	broad	very narrow conopeum-like structure obscured by a pocket-like silica flap	narrow, heavily silicified obscured by linear silica flange	absent
External fistula opening	obscured by a pocket-like silica flap	teardrop-shaped domed hymen	transapically elongated, partially obscured by two silica flanges	nearby circular domed hymen	domed oval hymen	obscured by linear silica flange
Internal fistula occlusion	nearly circular domed hymen	large, elliptical domed hymen supported by a series of stellately arranged struts	2–5 circular openings occluded by domed hymenes	junction of the lateral extension of the central nodule and the valve face	junction of the lateral extension of the central nodule and the valve face	domed oval hymen
Internal fistula opening location	close to the axial area, not reaching the axial rib	junction of the axial rib and the valve face	expansion of the central nodule	slightly raised rounded or nodular	knob-like, pointed	junction of the lateral extension of the central nodule and the valve face
Internal central thickening	wafer-like, with a small blunt tip	ridge-like, rounded and oblate	elongated, with a small pointed tip	up to 4, transapically elongated	numerous, elongated or circular up to 3	knob-like, pointed
Apical areola	1, slit-like, on the primary side	up to 4, irregular, on the primary side	up to 6, transapically elongated	up to 4, transapically elongated	up to 3	knob-like, pointed
Areolae in the terminal raphe fissure	up to 2	up to 3	up to 2	up to 3	up to 3	knob-like, pointed
Cingulum areolae density (in 1 μm)	~7	~6	~5	~6	~5	knob-like, pointed
Host organism	seagrass <i>Thalassia testudinum</i> blades	green turtle, Kemp's ridley, loggerhead, barnacle <i>Chelonibia testudinaria</i>	green turtle, Kemp's ridley, loggerhead, olive ridley, barnacles <i>Chelonibia testudinaria</i> and <i>Platylepas cornicata</i>	green turtle, loggerhead, barnacle <i>Chelonibia testudinaria</i>	green turtle, loggerhead, barnacle <i>Chelonibia testudinaria</i>	green turtle, loggerhead, barnacle <i>Chelonibia testudinaria</i>



**Figs 23–37.** *Proschkinia maluszekiana*. **Figs 23–26.** Light micrographs showing frustules with partially detached or missing valves. **Fig. 24.** Specimen showing the rimmed central raphe endings (arrowheads) and fistula opening (arrow). **Figs 27–37.** Scanning electron micrographs. **Fig. 27.** Detail of the apex showing two small areolae at the end of the terminal raphe fissure (arrowheads). **Fig. 28.** Apical part of the valve (external view). **Fig. 29.** Specimen with partially detached valves. Arrows indicate elongated areolae present at the valve apices. **Fig. 30.** External view of the central part of the valve with four rounded pores adjacent to each of the striae bordering the central area (arrowheads). **Fig. 31.** External view of the central part of the valve with broken conopeum revealing the central longitudinal rows of large rectangular areolae. **Fig. 32.** External view of the valve. **Fig. 33.** Internal view of the apical part of the valve showing the curved thickening (arrowheads) with a single areola at its end (arrow). **Fig. 34.** Internal view of the valve. Arrowheads indicate four pores adjacent to each of the complete central striae on both sides of the raphe occluded by rounded domed hymenes. **Fig. 35.** Eroded frustule revealing internal perforations on the folded girdle bands. **Figs 36, 37.** Internal view of the central part of the valve with partially eroded occlusion of the fistula revealing a series of supporting stellately arranged struts and four pores with rounded domed hymenes (arrows). Scale bars: Figs 23–26: 10 µm, Figs 29, 32, 34, 35: 5 µm, Figs 28, 30, 31, 33, 36, 37: 1 µm, Fig. 27: 500 nm.

with a few irregular areolae embedded within the fissure or directly next to the end of the shortened hook (Fig. 27, arrowheads). At the apices, several irregularly shaped areolae present (Figs 27–29, 32).

**Internal view:** Striae extending from the narrow pore-free zone on the mantle to the prominent and thicker (in its middle part) raphe-sternum (Figs 33, 34, 36, 37). Striae composed of square to rectangular areolae occluded by hymenes. First row of areolae, located closest to the raphe-sternum much larger, transapically elongated and distinctly raised (Figs 33, 34, 36, 37). Fistula occluded by one large, elliptical and clearly convex hymen supported by a series of stellately arranged struts (Figs 34, 36, 37). Additionally, four pores adjacent to each of the complete central striae on both sides of the raphe occluded by rounded domed hymenes (Figs 34, arrowheads, 36, arrows, 37, arrows). Raphe slit opening laterally in the raised raphe-sternum (Figs 33, 34, 36, 37). Central raphe endings very slightly expanded, slightly deflected towards the fistula (Figs 36, 37). An elongated, laterally protruding silica thickening with a small pointed tip present on the raphe-sternum, located between the central raphe endings (Figs 34, 36, 37). Terminal raphe endings elongated, lying somewhat laterally within the sternum, terminating onto small, simple helictoglossae, merging with slight thickenings corresponding to the terminal raphe fissures on the external surface of the valve (Fig. 33, arrowheads). Areolae at the end of the curved thickenings (Fig. 33, arrow) and those at the apices occluded by hymenes (Fig. 33).

Cingulum composed of multiple open copulae (Figs 29, 35). Pars interior with a row of hymenate, rectangular pores (Fig. 35), ca. 5 in 1 µm. Pars exterior plain (Fig. 29).

**Taxonomic remarks:** *P. maluszekiana* is the largest of the six newly described species (Table 2). It bears some resemblance to *P. complanata* but differs from the latter in possessing a well-defined, strongly asymmetrical central area with clearly convergent striae in the valve middle and a more prominent fistula occlusion when observed using LM (compare with Witkowski *et al.*, 2000, Plate 147, fig. 9). Specimens of *P. complanata* shown by Cox (2012; figs 11c and 11d) differ from *P. maluszekiana* in lacking the central longitudinal silica strips and the silica rims around both the central raphe endings and the external opening of the fistula. Furthermore, the internal thickening of the central nodule in *P. complanata* is small and slightly raised (resembling that observed in *P. sulcata*), whereas in *P. maluszekiana* it is much larger, elongated and with a pointed tip (Cox, 2012; fig. 15f). Although valve dimensions of *P. maluszekiana* overlap with those of *P. torquata*, the two species can be distinguished by, for instance, clear differences in the internal fistula

occlusion (large, elliptical domed hymen in *P. maluszekiana* and a series of 2–5 circular openings occluded by domed hymenes in *P. torquata*; Table 2). However, due to a relatively low resolution achievable with LM the fistula shape of the two species may be indistinguishable, and thus other features such as a larger and better-defined central area in *P. maluszekiana*, should be analysed and compared in LM-based analyses.

**HOLOTYPE:** Permanent slide BR-4560 and unmounted material deposited in the BR-collection housed by Botanic Garden Meise, Belgium.

**ISOTYPE:** Permanent slide SANDC-ST003 and unmounted material (sample ZA0762D/ZA0763D) deposited in the South African Diatom Collection housed by North-West University, Potchefstroom, South Africa.

**PARATYPES:** Permanent slide SANDC-TPD05-18 and unmounted material (sample TPD-05) deposited in the South African Diatom Collection housed by North-West University, Potchefstroom, South Africa, and the permanent slide TPD-05-16 deposited at the Yale Peabody Museum of Natural History, New Haven, USA.

**TYPE LOCALITY:** Kosi Bay, South Africa (26°59'39"S, 32°51'60"E). Collected from the carapace of the adult female loggerhead *Caretta caretta* (tag numbers: ZA0762D, ZA0763D) by R. Majewska, 15 December 2017 (holotype).

Riverhead, New York, USA. Taken from the carapace of a juvenile Kemp's ridley *Lepidochelys kempii* found cold-stunned (and beyond rehabilitation) on the beach by an anonymous collector, 20 December 2012 (paratype).

**ETYMOLOGY:** The epithet honours Ms Alina Maluszek (The II 'Mikolaj Kopernik' Secondary School in Leszno, Poland), the species author's early biology teacher, first mentor, and ongoing inspiration, in recognition of her dedication to teaching and the invaluable work of all secondary school teachers.

**ECOLOGY:** Epizoic on juvenile Kemp's ridleys *L. kempii* and a juvenile green turtle *Chelonia mydas* from Long Island (New York, USA), and on adult female loggerheads *C. caretta* and barnacles *Chelonibia testudinaria* collected from loggerheads from Kosi Bay (South Africa).

### *Proschkinia sulcata* Majewska, Van de Vijver & Bosak, sp. nov. (Figs 38–51)

**Light microscopy:** (Figs 38–42): Frustules in girdle view broad with numerous girdles bands (Figs 38–40). Valves narrowly lanceolate with elongated acutely rounded to very slightly rostrate apices (Figs 38–42). Valve dimensions ( $n = 30$ ): length 10–28 µm, width 2.5–4 µm, length/width ratio 4.0–7.4. Axial area

narrow, with prominent raphe-sternum (Figs 38–42). Central area barely distinguishable, with two central striae more widely spaced and visible (Fig. 40, arrowheads). Other striae indiscernible. Fistula visible as glistening dot in the central area (Fig. 41, arrow). Girdle bands open, appearing unornamented (Figs 38–41).

*Scanning electron microscopy* (Figs 43–51). *External view:* Valve face flat. Several distinct longitudinal cord-like silica strips running from apex to apex. Near the axial area and close to the valve face/mantle junction, strips occasionally interrupted (Figs 43–47). Mantle shallow, unperforated. Very narrow pore-free border running entirely around the valve at the valve face/mantle junction (Fig. 44, arrowheads). Striae uniserial, barely visible between the longitudinal silica strips, parallel to weakly convergent at the apices (Figs 43, 46), 40–45 in 10 µm. Areolae rectangular, more or less uniform in size (Figs 43, 46, 47). Raphe branches straight, running between two raised silica ridges developing into a very narrow conopeum-like structure (Figs 43, 45–47). Central raphe endings straight, slightly expanded, with raised silica rims creating spatulate openings, clearly deflected towards the secondary side of the valve (away from the fistula; Figs 45–47). Fistula mostly hidden beneath the pocket-like thickening (formed by the fusion of longitudinal silica strips) with linear opening parallel to the raphe-sternum (Figs 45–47). Terminal raphe fissures strongly hooked towards the secondary side of the valve (Figs 43–45), with up to three small areolae at the end of the fissure (Fig. 43, arrowheads). Several apically elongated to irregularly shaped areolae present at the valve apex perpendicular to the valve margin (Fig. 45).

*Internal view:* Striae parallel becoming slightly convergent towards the apices (Figs 48–50), composed of square areolae, occluded by perforated hymenes. Areolae uniform in size across the valve face, only slightly larger and slightly raised close to the raphe-sternum (Figs 48–50). Fistula occluded by one domed hymen forming a ball-like structure, not reaching the raphe-sternum (Figs 49, 50). Raphe slit opening laterally onto the uniformly thick raphe-sternum towards the secondary side (Figs 48–50). Central raphe endings very slightly expanded, slightly deflected towards the fistula (Figs 49, 50). A lateral and slightly raised rounded or nodular thickening present on the raphe-sternum, between the central raphe endings (Figs 49, 50). Terminal raphe endings straight, lying somewhat laterally on the sternum, terminating onto simple helictoglossae (Figs 48, 49). Thickenings corresponding to the hooked external terminal raphe fissures present poleward from the helictoglossae (Figs 48, 49, arrowheads). Areolae at the apices (Fig. 48, arrow) and those at the end of the

curved thickenings (Fig. 48, arrowheads) occluded by slightly raised hymenes.

Cingulum composed of multiple open copulae (Figs 44, 51). Pars interior with a row of hymenate, rectangular pores (Fig. 51); ca. 6 in 1 µm. Pars exterior plain (Fig. 44).

*Taxonomic remarks:* *P. sulcata* resembles *P. browderiana* in having a similar valve outline (lanceolate with rounded to slightly rostrate apices), mostly uninterrupted, longitudinal cord-like silica strips on the valve face, and fistula externally obscured by a pocket-like silica flap and internally occluded by a domed rounded hymen (Table 2). However, the cord-like silica strips in *P. sulcata* are narrower and more irregular than those in *P. browderiana*, and do not reach the distinct valve face-mantle junction creating a smooth, pore-free margin around the valve face. The internal fistula occlusion in *P. sulcata* lies on the junction of the lateral extension of the central nodule, whereas in *P. browderiana* it does not reach the sternum (Table 2). Furthermore, the two species differ in the shape of the internal central thickening (slightly raised rounded or nodular in *P. sulcata* and wafer-like, with a small blunt tip in *P. browderiana*) and the number of apical areolae (up to four in *P. sulcata* and always one, slit-like, on the primary side, in *P. browderiana*; Table 2).

**HOLOTYPE:** Permanent slide BR-4561 and unmounted material (sample ‘Palma Modesty’) deposited in the BR-collection (Belgium).

**ISOTYPE:** Permanent slide HRNDC000007 deposited in the Croatian National Diatom Collection housed by Faculty of Science, University of Zagreb, Croatia.

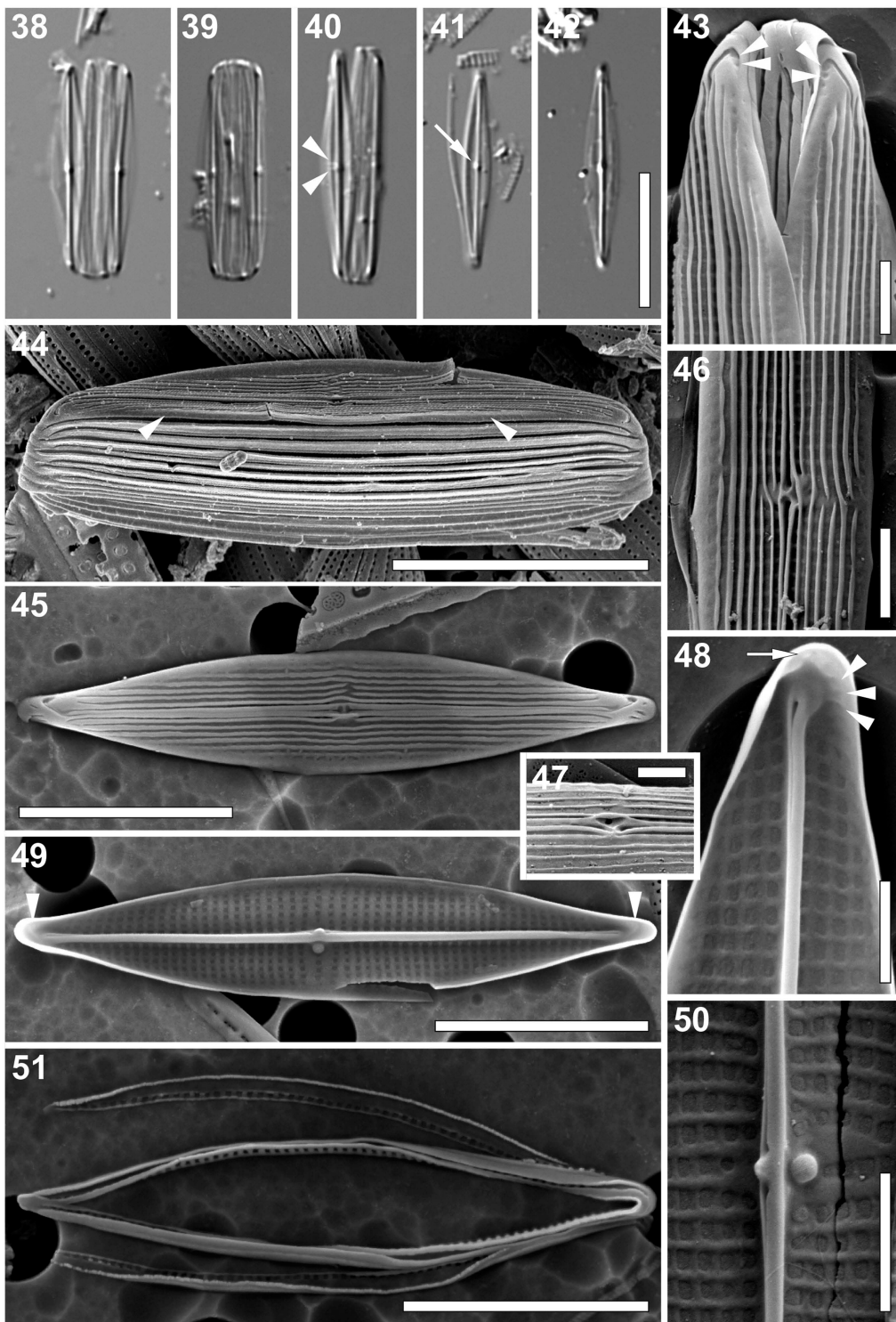
**PARATYPE:** Permanent slide SADC-ST003 deposited in the South African Diatom Collection housed by North-West University, Potchefstroom, South Africa.

**TYPE LOCALITY:** Marine Turtle Rescue Centre, Pula, Croatia (44°50'07"N, 13°49'58"E). Collected from a semi-adult (45 kg) female loggerhead turtle *Caretta caretta* named ‘Palma Modesty’ by K. Gobić Medica, 30 September 2016 (holotype).

Kosi Bay, South Africa (26°59'39"S, 32°51'60"E). Collected from the carapace of the adult female loggerhead *C. caretta* (tag numbers: ZA0762D, ZA0763D) by R. Majewska, 15 December 2017 (paratype).

**ETYMOLOGY:** From the Latin word *sulcata* (‘ploughed’), with reference to the external cord-like silica strips and grooves on the valve face.

**ECOLOGY:** Epizoic on carapaces of adult olive ridleys *Lepidochelys olivacea* from Ostional (Pacific coast of Costa Rica), adult loggerheads *C. caretta* from Adriatic Sea (Croatia), Kosi Bay (South Africa), Florida (USA) and South Carolina (USA), and on an adult hawksbill *Eretmochelys imbricata* from Hawaii (USA) as well as on skin and associated



**Figs 38–51.** *Proschkinia sulcata*. **Figs 38–42.** Light micrographs. **Figs 38, 40.** Frustules with partially detached valves. Arrowheads indicate the two more widely spaced central striae. **Fig. 39.** Girdle view. **Figs 41, 42.** Valve view. Arrow indicates the fistula visible as refractive dot. **Figs 43–51.** Scanning electron micrographs. **Fig. 43.** Apical part of the frustule showing series small areolae at the end of the terminal raphe fissures (arrowheads). **Fig. 44.** Intact frustule. Arrowheads indicate a subtle valve face-mantle junction. **Fig. 45.** External view of the valve. **Fig. 46.** Central part of the valve (external view). **Fig. 47.** Detail of the central area revealing the external fistula opening hidden beneath the pocket-like silica flap. **Fig. 48.** Internal view of the apical part of the valve showing a series of small areolae at the end of the curved thickening (arrowheads) and a single areola close to the apex margin (arrow). **Fig. 49.** Internal view of the valve with curved thickenings at the apices (arrowheads). **Fig. 50.** Central part of the valve (internal view). **Fig. 51.** Detached girdle bands. Scale bars: Figs 38–42, 44: 10 µm, Figs 45, 49, 51: 5 µm, Figs 43, 46–48, 50: 1 µm.

barnacles of loggerheads and leatherbacks *Dermochelys coriacea* from Kosi Bay (South Africa).

***Proschkinia torquata* Bosak, Van de Vijver & Majewska sp. nov. (Figs 52–65)**

*Light microscopy* (Figs 52–56): Frustules in girdle view rectangular with broadly rounded ends and numerous copulae (Fig. 52). Valves narrowly lanceolate with slightly protracted, cuneately rounded apices (Figs 53–56). Valve dimensions ( $n = 25$ ): length 21–32  $\mu\text{m}$ , width 3–5  $\mu\text{m}$ , length/width ratio 5.6–7.9. Axial area narrow, distinct raphe-sternum present (Figs 52–56). Striae very fine, barely discernible, 28–32 in 10  $\mu\text{m}$ , sparser, slightly convergent and clearly visible near the central area (Figs 52–56). Fistula transapically elongated (Figs 52–56). Central raphe endings evident on one side of the raphe-sternum (Fig. 56, arrowheads). Helictoglossae at the apices visible as refractive dots (Figs 55, 56). Girdle bands open, appearing unornamented (Figs 52–54).

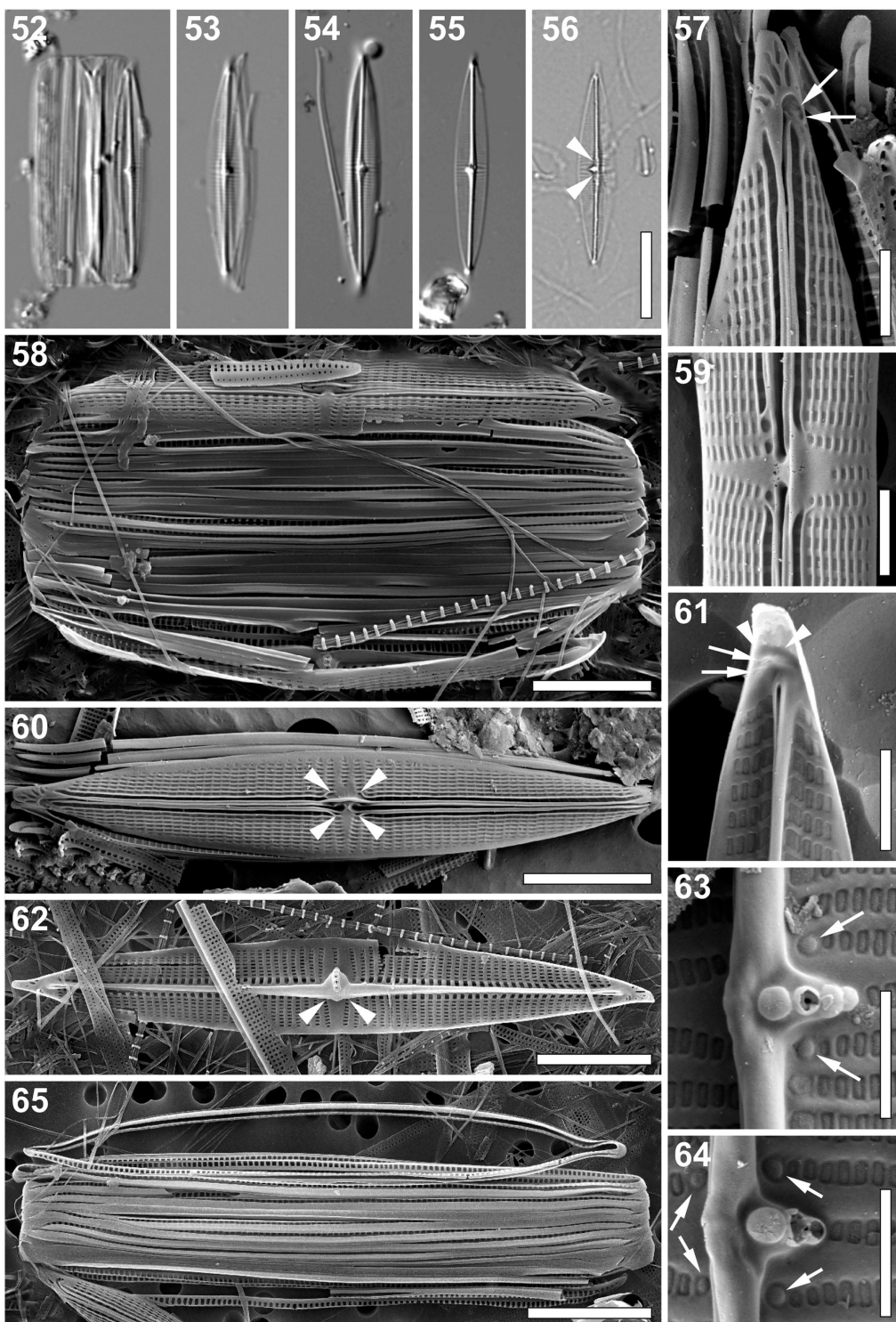
*Scanning electron microscopy* (Figs 57–65): *External view*: Valve face flat with slightly raised longitudinal silica strips interrupted at the central area running between the areolae, flattening near the valve margins (Figs 57–60). Mantle very shallow (Figs 58, 60). Clear pore-free zone running around the entire valve at the valve face/mantle junction (Figs 57–60). Striae uniserrate, parallel, becoming slightly convergent close to the apices and near the central area, composed of rectangular, apically elongated areolae (Figs 57–60). Areolae near the axial area larger, clearly sunken and partially covered by a narrow, heavily silicified conopeum with a single central groove (Figs 57–60). Areolae near the valve margin becoming smaller, getting an irregular shape (Figs 57, 58, 60). Raphe branches straight, partially obscured by the thickened rims of the conopeum (Figs 57–60). Central raphe endings elongated, slightly expanded, with a distinct silica rim, slightly deflected towards the fistula (Figs 59, 60). Terminal raphe fissures strongly hooked towards secondary side of the valve (Figs 57, 58, 60). Two or three irregular hymenate areolae embedded within hooks of the terminal raphe fissures (Figs 57, 58, arrows). Central area asymmetrical, V-shaped, with a single shortened stria on the primary side of the valve and a triangular pore-free area created by two convergent striae on the opposite side of the raphe (Fig. 59, 60). A pocket-like rimmed silica flap completely obscuring the fistula opening on the primary side of the valve (Figs 59, 60). Four roundish pores adjacent to the striae bordering the central area present, partially hidden under the silica rims extending from conopeum and the central longitudinal strips (Fig. 60, arrowheads). Apices with several

elongated, irregular areolae close to the valve margins poleward of the terminal fissures (Figs 57, 58, 60).

*Internal view*: Striae almost parallel extending from the pore-free mantle to the prominent raphe-sternum, composed of narrowly rectangular and apically elongated areolae (Figs 61–64). Areolae close to the raphe-sternum transapically elongated, much larger and raised (Figs 61–63). Raphe slit visible only at the apices, opening laterally on the raphe-sternum (Figs 61, 62). Central raphe endings covered by an elongated and somewhat flattened thickening of the central nodule extending laterally from the axial rib to the secondary side of the valve (Figs 62, arrowheads, 63, 64). Fistula located on lateral expansion of the central nodule showing a complex structure with a series of 2–5 circular openings occluded by finely perforated domed hymenes (Figs 62–64). Occlusions of the four pores adjacent to the central striae clearly rounded and domed (Figs 62, 63 arrows, 64 arrows). Terminal raphe endings slightly expanded, lying somewhat laterally on the sternum, terminating onto simple helictoglossae (Figs 61, 62). Thickening corresponding to the external raphe fissures present poleward from helictoglossae (Figs 61, arrowheads, 62). Two or three areolae at the end of the hooked thickenings (Fig. 61, arrows) and those at the apices (Fig. 61) occluded by weakly raised hymenes.

Cingulum consisting of multiple open copulae (Figs 57, 58, 60, 65), folded with the fold on the cell interior (Figs 58, 65). Pars interior with row of hymenate, rectangular, transapically elongated pores (Figs 57, 58, 60, 65), pore density ca. 5 in 1  $\mu\text{m}$ . Pars exterior plain (Figs 57, 58, 60, 65).

*Taxonomic remarks*: *P. torquata* and *P. complanatoides* are similar in their valve dimensions and shape. However, *P. torquata* differs from the latter in possessing longitudinal silica strips over the central part of its valve face and the external fistula opening obscured completely by a pocket-like rimmed silica flap. Moreover, the internal opening of the fistula in *P. torquata* is composed of 2–5 circular domed hymenes raised on the lateral expansion of the central nodule, whereas in *P. complanatoides* the opening is covered by a linear structure that lies flat on the valve face (Zgrundo *et al.*, 2013). Although *P. complanatoides* is often recorded in floristic surveys worldwide, suggesting it is a cosmopolitan taxon (Lobban *et al.*, 2012; Pezzolesi *et al.*, 2017; Pichierri *et al.*, 2017; Sempere-Valverde *et al.*, 2018), images of the specimens observed are rarely provided and it is likely that the current perception of the species' biogeography is affected heavily by misidentification and forced-fitting. Specimens of *Navicula complanatoides* shown in Brogan & Rosowski (1988) differ from both



**Figs 52–65.** *Proschkinia torquata*. **Figs 52–56.** Light micrographs. **Fig. 52.** Specimen in girdle view with partially detached valve. **Figs 53–56.** Valve view. Arrowheads indicate the visible central raphe endings. **Figs 57–64.** Scanning electron micrographs. **Fig. 57.** External view of the apical part of the valve with several irregular areolae embedded within the terminal raphe fissure (arrows). **Fig. 58.** Frustule with partially detached valves. **Fig. 59.** Central part of the valve (external view). **Fig. 60.** External view of the valve. **Fig. 61.** Internal view of the apical part of the valve showing two small areolae (arrows) at the end of the curved thickening (arrowheads). **Fig. 62.** Internal view of the valve. Arrowheads indicate an elongated thickening of the central nodule extending laterally from the axial rib to the secondary side of the valve obscuring the central raphe endings. **Figs 63, 64.** Internal view of the central part of the valve with pores with rounded domed hymenes adjacent to each of the complete central striae on both sides of the raphe (arrows). **Fig. 65.** Detached girdle bands showing the transapically elongated pores on the internal side. Scale bars: Figs 52–56: 10 µm, Figs 58, 60, 62, 65: 5 µm, Figs 57, 59, 61, 63, 64: 1 µm.

the lectotype and *P. torquata* in, for instance, possessing numerous, uninterrupted cord-like silica strips on the valve face. Karayeva & Bukthiyarova (2010) presented several SEM images of a taxon (identified by the authors as *P. complanatoides*) found on the eastern and southern coasts of the Caspian Sea that shows some striking similarities (e.g. fistula externally covered by a pocket-like rimmed silica flap and internally occluded by a series of domed hymenes) to *P. torquata*, and may in fact be conspecific with the new taxon described here. Specimens observed by Lobban *et al.* (2012) in the vicinity of Guam lack the central area due to uniformly spaced, almost perfectly parallel striae and possess an internal fistula occlusion composed of at least six small, densely packed circular structures, and probably belong to a yet undescribed *Proschkinia* species.

**HOLOTYPE:** Permanent slide BR-4562 and unmounted material (sample ‘Palma Modesty’) deposited in the BR-collection (Belgium).

**ISOTYPES:** Permanent slide HRNDC000007 deposited in the Croatian National Diatom Collection housed by Faculty of Science, University of Zagreb, Croatia.

**PARATYPE:** Permanent slide SADC-ST004 deposited in the South African Diatom Collection housed by North-West University, Potchefstroom, South Africa.

**TYPE LOCALITY:** Marine Turtle Rescue Centre, Pula, Croatia (44°50'07"N, 13°49'58"E). Collected from a semi-adult (45 kg) female loggerhead *Caretta caretta* named ‘Palma Modesty’ by K. Gobić Medica, 30 September 2016 (holotype).

Kosi Bay, South Africa (27°00'29"S, 32°52'49"E). Collected from the barnacle *Platylepas coriacea* growing on the adult female leatherback *Dermochelys coriacea* (tag numbers: ZATT559, ZAST653) by C. Nolte, 8 January 2016 (paratype).

**ETYMOLOGY:** From the Latin word *torquata* (‘wearing a necklace’), with reference to the internal fistula occlusion resembling a necklace with 2–5 beads.

**ECOLOGY:** Epizoic on carapaces of adult loggerheads *C. caretta* from Adriatic Sea (Croatia) and Kosi Bay (South Africa), and on sea turtle-associated barnacles *Chelonibia testudinaria* growing on adult loggerheads from Kosi Bay (South Africa).

#### *Proschkinia vergostriata* Frankovich, Ashworth & M.J.Sullivan, sp. nov. (Figs 66–78)

**Light microscopy (Figs 66–69):** Frustules in girdle view small, weakly silicified, rectangular with rounded ends and numerous copulae (Figs 66, 67). Frustule width 3.5–7.5 µm ( $n = 30$ ). Valves narrowly lanceolate with weakly protracted, cuneate substrate apices (Figs 68, 69). Valve dimensions ( $n =$

30, natural and cultured populations): length 5.0–15.0 µm, width 1.5–3.0 µm, length/width ratio 3.9–6.2. Axial area very narrow with a distinct raphe-sternum (Fig. 68, arrow). Fistula evident in the central area (Fig. 69, arrow). Striae discernible near the central area, gradually becoming undiscernible towards apices, slightly convergent (Figs 66–69).

**Scanning electron microscopy (Figs 70–78): External view:** Valve face flat. Longitudinal silica strips absent. Striae uniserial, their density often increasing towards the apices by up to 40%, 27 (central area)–43 (apex) in 10 µm. Striae composed of large rectangular areolae, decreasing in size towards the axial area (Figs 70–73), ca. 60 in 10 µm. Areolae adjacent to the raphe distinctly larger, clearly sunken (Figs 70–73). Striae nearly parallel at the central area becoming rapidly curved and strongly convergent towards the apices (Figs 70–73), continuing onto the mantle (Figs 70, 71). Mantle shallow, lacking a clear valve face/mantle junction (Figs 70, 71). Raphe located between very narrow silica ridges, weakly raised in the valve middle (Figs 70–73). Central area rectangular, almost symmetrical, formed by 1–2 shortened striae on each side of the raphe-sternum (Figs 71–73). Central raphe endings closely spaced, spatulate, slightly bent towards the secondary side of the valve (Figs 72, 73). Linear silica flange present next to the central area on the primary side of valve forming a hood, obscuring the external fistula opening (Fig. 72, arrow). Terminal raphe fissures strongly hooked towards the secondary side, extending onto the valve mantle (Fig. 70). Single, transapically elongated areola at the end of the hooked raphe fissures (Fig. 70, arrow). Unornamented areas on each hemivalve adjacent to polar raphe endings extending onto mantle margins (Figs 70, 71). Single row of apically elongated pores at apices poleward of polar raphe endings and unornamented areas (Figs 70, 71, 73).

**Internal view:** Areolae squarish to elliptical, gradually decreasing in size towards the raphe-sternum, except for the central longitudinal row adjacent to the axial area composed of much larger, rounded areolae, clearly raised on the raphe sternum (Figs 74–76, 78). Raphe slit visible only at the central endings and the apices, opening laterally within a thick axial rib (Figs 74–76, 78). Central raphe endings simple, bent towards the fistula (Figs 75, 76, 78). A small knob-like pointed structure protruding laterally from the central nodule, opposite to the fistula (Figs 75, 76, 78). Internal fistula opening visible as a lateral expansion of the central nodule, covered by a domed oval structure (Figs 75, 78) but missing in some specimens (Fig. 76). Simple helictoglossae present at the thickened apices (Figs 74, 75). Isolated areolae occluded by hymenes poleward of the helictoglossae (Fig. 74).

Cingulum composed of multiple open copulae (up to 16 observed; Figs 71, 77). Unperforated pars exterior of

copulae overlapping the perforated pars interior of adjacent copulae producing an external appearance of the cingulum as unperforated bands (Figs 71, 77). Separated copulae revealing single row of rectangular pores on the pars interior (Fig. 77), ca. 4 in 10 µm.

**Taxonomic remarks:** *P. vergostriata* and *P. lacrimula* are the only species of the genus lacking longitudinal silica strips on their valve face (Table 2). *P. vergostriata* and *P. lacrimula* are both very small diatoms ( $\leq 15 \mu\text{m}$ ) and both live epizoically on sea turtles from the north-western Atlantic Ocean (Table 2). These species can be distinguished by differences in stria structure, areola shape and external fistula morphology. *P. vergostriata* has strongly curved and divergent striae, broadly rectangular areolae, and fistula with external opening obscured by a linear silica flange. In contrast, *P. lacrimula* has striae that are nearly parallel throughout sometimes becoming slightly convergent at the apices, narrow apically elongated linear areolae, and the external opening of the fistula is a simple unobscured pore (Table 2).

**HOLOTYPE:** Permanent slide BR-4563 and unmounted material deposited in the BR-collection housed by Botanic Garden Meise, Belgium.

**ISOTYPES:** Permanent slide SANDC-ST005 deposited in the South African Diatom Collection housed by North-West University, Potchefstroom, South Africa and permanent slide DH 311960 and unmounted material DH 311961 deposited in the Academy of Natural Sciences of Drexel University, Philadelphia, Pennsylvania, USA.

**TYPE LOCALITY:** The Turtle Hospital, Florida Bay, Florida, USA ( $24^{\circ}42'41''\text{N}$ ,  $81^{\circ}06'04''\text{W}$ ). Collected from the neck skin of a captive rehabilitating green sea turtle *Chelonia mydas* by T.A. Frankovich, 24 May 2016.

**ETYMOLOGY:** From the Latin words *vergo* ('to slope back') and *striata* ('grooves'), with reference to the curved, convergent striae.

**ECOLOGY:** Epizoic on skin of loggerheads *Caretta caretta* and green turtles *C. mydas* from Florida Bay, Florida (USA).

### Molecular phylogenetic analysis

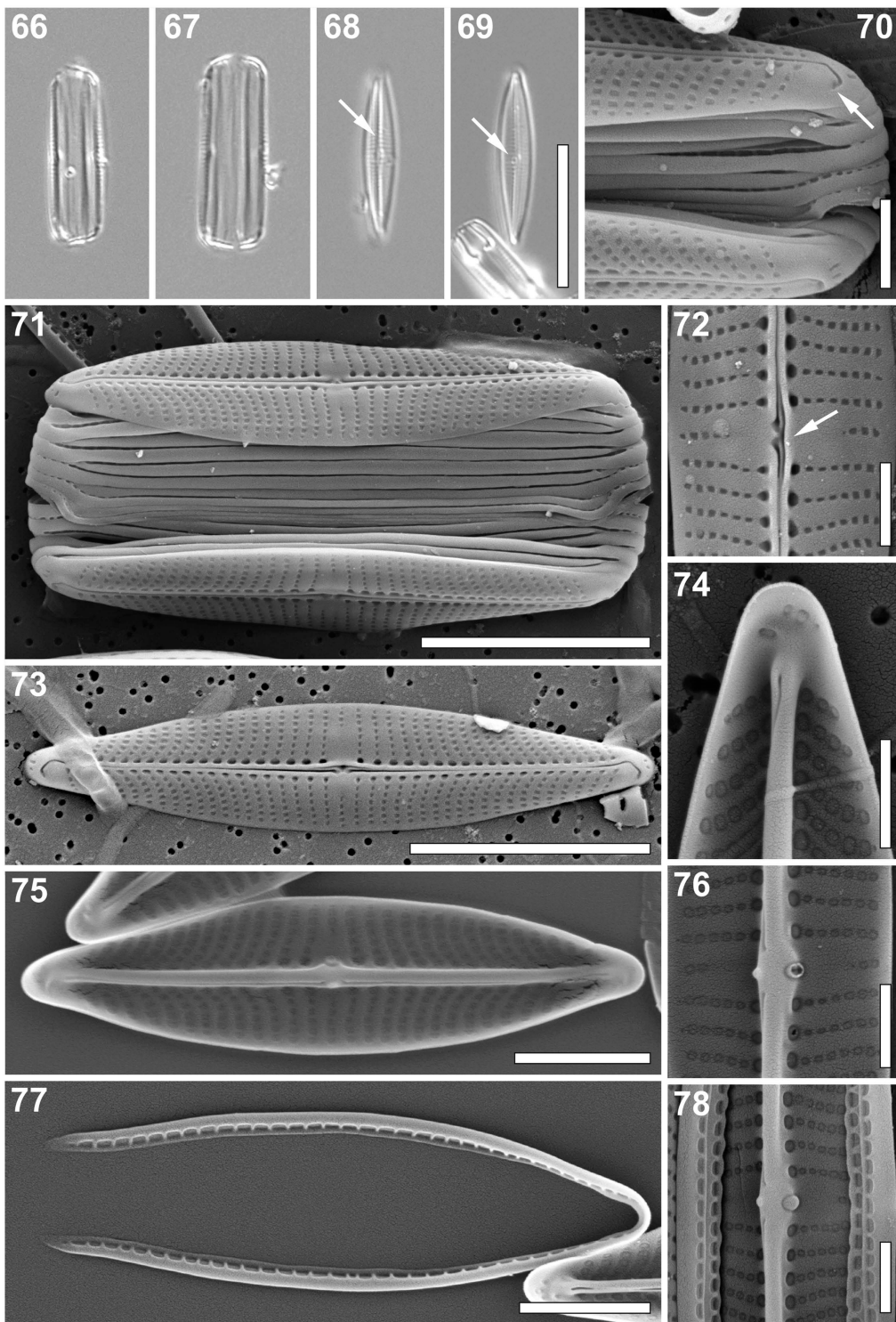
The best tree found from the ML 3-gene phylogenetic analysis is presented in Supplementary figs S2, S3, with the clades relevant to the placement of *Proschkinia* presented in Fig. 79. The MP analysis of the same dataset resolved a total of 28 equally parsimonious trees, each with a total length of 23 317 steps, consistency index of 0.11 and retention index of 0.58. The strict consensus tree (Supplementary fig. S4) calculated from these equally parsimonious trees collapsed 42 nodes. The *Proschkinia* strains were monophyletic, with strong support (bootstrap

support [bs] = 93% MP, 80% ML), sister to the *Fistulifera* clade (bs = 100% MP and ML). Epizoic *P. vergostriata* were monophyletic (bs = 80% MP, 100% ML), sister to an epiphytic *P. cf. complanatula* strain isolated from the central California coast (bs = 90% MP, 80% ML; see Supplementary figs S3, S4). Within *P. vergostriata*, strains grouped by collection site under the ML criterion, either a green sea turtle sampled in a rescue facility (HK548, HK549, HK550) or a loggerhead turtle sampled from Florida Bay (HK551, HK552). Under the MP criterion, however, this grouping could not be resolved.

### Discussion

Based on the morphological analyses of a large number of specimens ( $> 200$ ) and samples ( $> 100$ ), we believe that the six species presented here belong to the genus *Proschkinia*. All new taxa share features typical of the genus, such as a lanceolate to linear-lanceolate valve outline, numerous U-shaped open girdle bands with perforations on the internal part of the fold, and a fistula with a single external opening and domed, sometimes multiple internal occlusions. They also possess a lateral internal thickening of the central nodule that varies in shape and size among species, elongated or irregular apical areolae beyond the terminal raphe fissures and small areolae embedded within those fissures (to the best of our knowledge this last character has not been observed in other diatom genera). Although *Proschkinia* species are often reported from various ecological and floristic surveys conducted around the globe (e.g. Cholnoky, 1963; Ehrlich, 1978; Lange & Tiffany, 2002; Lobban *et al.*, 2012) and they probably constitute a common component of benthic brackish and marine biofilms, few images of the observed specimens are available so it is probable that the species diversity within *Proschkinia* is much higher than currently reported. Similarly, investigations exploring the ultrastructure of *Proschkinia* frustules are rare, and it is conceivable that our understanding of both the morphology and physiological function of their various siliceous structures will improve with further observations utilizing advanced microscopy techniques. The new species clearly differ from each other and can be easily distinguished using SEM, allowing a thorough analysis of all distinct characters (Table 2). Using LM, partially due to weak frustule silicification, proper identification may prove more difficult as taxonomically important features such as fistula shape or presence of a conopeum and longitudinal silica strips on the valve face surface may remain unresolved.

A 3-gene phylogenetic analysis indicated that epizoic *P. vergostriata* strains were sister to non-epizoic *P. cf. complanatula*, forming a monophyletic clade and thus confirming further the identity of the former as a *Proschkinia* species. Moreover, the analysis



**Figs 66–78.** *Proschkinia vergostriata*. **Figs 66–69.** Light micrographs. **Figs 66, 67.** Girdle view. **Figs 68, 69.** Valve view. Arrows indicate a distinct raphe-sternum (Fig. 68) and the fistula (Fig. 69). **Figs 70–78.** Scanning electron micrographs. **Fig. 70.** Apical part of the frustule showing a single transapically elongated areola at the end of the terminal raphe fissure (arrow). **Fig. 71.** Complete frustule. **Fig. 72.** Central part of the frustule showing a silica flange obscuring the external fistula opening (arrow). **Fig. 73.** External view of the valve. **Fig. 74.** Internal view of the apical part of the valve. **Fig. 75.** Internal view of the valve. **Fig. 76.** Internal view of the valve centre with missing fistula occlusion. **Fig. 77.** Detached girdle band. **Fig. 78.** Internal view of the valve centre. Scale bars: Figs 66–69: 10 µm, Figs 71, 73: 5 µm, Figs 75, 77: 2 µm, Figs 70, 72, 74, 76, 78: 1 µm.

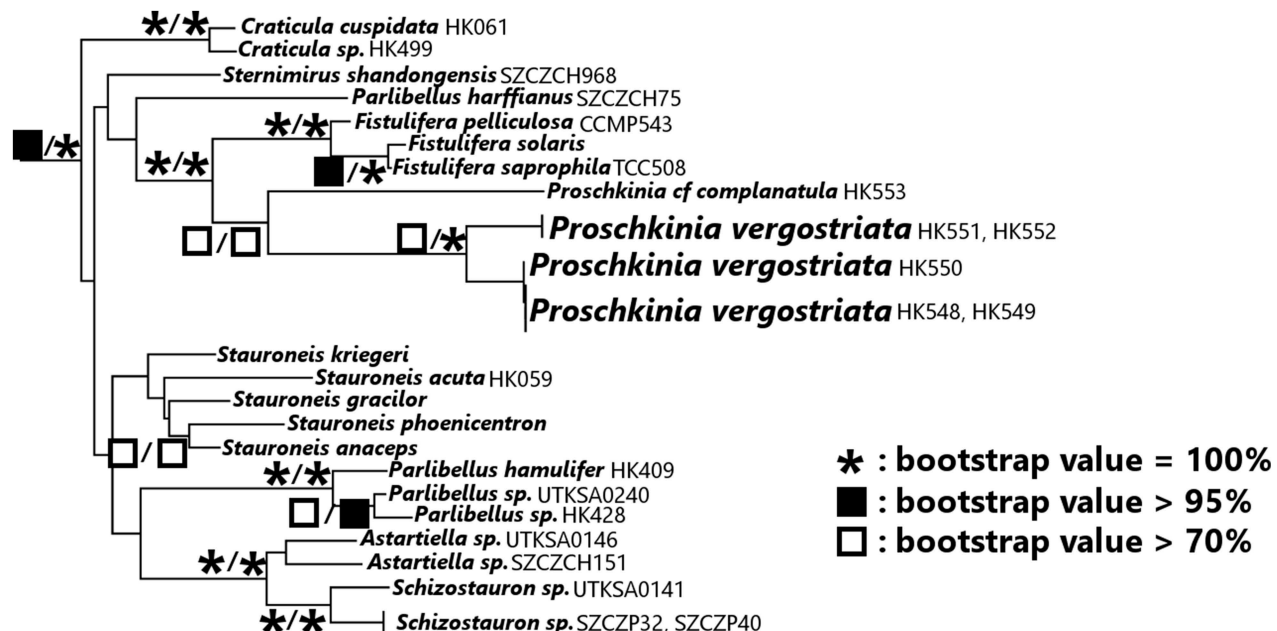


**Fig. 79.** Maximum likelihood (ML) phylogram based on the 3-gene dataset (nuclear-encoded ribosomal SSU, chloroplast-encoded *rbcL*, *psbC* markers). Characters representing three categories of bootstrap values from 1000 pseudoreplicates (100%, >95%, >70%) for both maximum parsimony (MP) and ML analyses are found over the corresponding nodes (MP/ML). Only the clade of raphid diatoms containing *Fistulifera* and *Proschkinia* is presented in this figure for clarity. The ML tree presents raphid diatoms only, and the ML tree presenting the complete taxon sampling and the MP tree presenting the complete taxon sampling can be viewed in the Supplementary figs S2, S3 and S4, respectively.

confirmed a close relationship of *Proschkinia* and *Fistulifera* as was previously indicated by Gastineau *et al.* (2019), but with a much more diverse assemblage of taxa in the dataset, which might influence our interpretation of the resulting tree. For example, one may be tempted to draw conclusions about a potential homology between the fistula of *Proschkinia* and *Fistulifera* and the internally occluded stigma of *Didymosphenia geminata*, which was sister to the *Proschkinia*+*Fistulifera* clade in the dataset presented by Gastineau *et al.* (2019). This, however, is not supported by our dataset with expanded taxon sampling.

*P. lacrimula* and *P. vergostriata* are currently the smallest known members of the genus with valves not exceeding 15 µm. As indicated by recent reports (Frankovich *et al.*, 2016; Majewska *et al.*, 2018a,b; Riaux-Gobin *et al.*, 2017a,b; Kaleli *et al.*, 2018), small size is typical of several other taxa described from sea turtles (e.g. *Chelonicola*, *Medlinella*, *Labellicula*, *Poulinea*) and may constitute an important adaptation to an epizoic lifestyle. Although all new *Proschkinia* species described here were found on the surface of living marine organisms (sea turtles, sea turtle-associated barnacles or seagrasses), it is presently unclear whether these are exclusively epibiotic taxa. Interestingly, four (*P. lacrimula*, *P. maluszekiana*, *P. sulcata* and *P. vergostriata*) out of five sea turtle-associated *Proschkinia* species were found on at least two different sea turtle species, whereas three species (*P. maluszekiana*, *P. torquata* and *P. sulcata*) were found on sea turtles from at least two different continents. This observation may

suggest that the newly described species are well-adapted to epizoic growth and may be a consistent element of sea turtle-associated diatom communities across the oceans. On the other hand, the presence of *P. browderiana* in seagrass samples and its absence in sea turtle material (including juvenile green turtles that are known to feed on *T. testudinum*, Bjorndal, 1980) collected from the same area indicate a certain degree of substratum preference within epibiotic *Proschkinia* members.

*P. maluszekiana*, *P. sulcata* and *P. torquata* were found on both sea turtles and sea turtle-associated barnacles. Although diatoms on the latter are rarely analysed, recent observations suggest that diatom diversity on sea turtle barnacles may be much higher than on sea turtle carapace or skin (R. Majewska, unpubl.). Possessing motile and pelagic larval stages, barnacles (such as the cosmopolitan *Chelonibia testudinaria*; Zardus & Hadfield, 2004) may serve as an important vector for sea turtle diatom dispersal among various sea turtle individuals, sea turtle species and possibly other marine vertebrates. Further research here may shed more light on epizoic diatom colonization strategies and expand our knowledge on epizoic biofilm formation.

Very recently a new species of *Craspedostauros*, *C. alatus*, has been described from frozen specimens of sea turtles deposited at the Peabody Museum of Natural History, USA (Majewska *et al.*, 2018a). The current paper is thus the second describing a new diatom species (*P. lacrimula*) from the museum sea turtle specimens, further supporting the hypothesis that zoological museum collections may constitute an

important source of both epizoic diatom specimens and information on their biogeography and substratum preferences. However, as previously indicated, several limitations of the approach must be considered (Majewska *et al.*, 2018a). Further analyses are required to assess the potential for sonication to break diatom valves during their extraction from the animal sample and optimize the duration and intensity of sonication as a method of detaching intact diatoms from their substratum.

## Acknowledgements

We thank Diane Z. M. Le Gouvello du Timat, Anthony Evlambiou, Wynand van Losenoord (Nelson Mandela University, South Africa), Karin Gobić Medica (Aquarium Pula, Croatia) and Tilen Genov (Morigenos, Slovenia) for their invaluable help during the material collection. Lourdes Rojas (Peabody Museum of Natural History, USA) assisted in diatom extraction from the sea turtle museum specimens, Anatolyi Levanets (North-West University, South Africa) helped translate some of the Russian articles used in this study, Edward C. Theriot (The University of Texas at Austin, USA) assisted and advised the phylogenetic analyses, and Klara Filek (University of Zagreb, Croatia) isolated the strain of *P. sulcata* (TB0019). We are also grateful to Richie Moretti and Bette Zirkelbach (The Turtle Hospital, Marathon, USA) for generously providing access to sea turtles in their care, Ania Wachnicka (The South Florida Water Management District, USA) for collecting material from Biscayne Bay, Nicole Stacy (University of Florida, USA) for assistance in obtaining epizoic materials, and Robert A. DiGiovanni, Jr. (Atlantic Marine Conservation Society, USA), the former director of the Riverhead Foundation for Marine Research and Preservation, USA, for the donation of several sea turtle carcasses used in this study to the Peabody Museum of Natural History. Samples were collected under permit MTP 15-021.

## Disclosure statement

No potential conflict of interest was reported by the authors.

## Funding

This work was done with partial financial support from The Systematics Association (UK) through the Systematics Research Fund Award granted to R. Majewska (2017), the Croatian National Fund under the project UIP-2017-05-5635 (TurtleBIOME), and the National Oceanic Atmospheric Administration under the project AWD00000006263. This is contribution #129 from the Center for Coastal Oceans Research in the Institute of Water and Environment at Florida International University.

## Supplementary information

The following supplementary material is accessible via the Supplementary Content tab on the article's online page at <https://doi.org/10.1080/09670262.2019.1628307>

**Supplementary table S1.** Taxa, strain voucher ID, and GenBank accession numbers for strains used in the DNA sequence data phylogenetic analysis. Collection site for sample of original strain isolation is also included (where known); in the case of cultures from public collections, the culture ID is provided in this column (UTEX = UTEX Culture Collection of Algae; NCMA = National Center for Marine Algae and Microbiota; CSIRO = Australian National Algae Culture Collection; MCC-NIES = Microbial Culture Collection at National Institute for Environmental Studies). Ingroup taxa (raphid pennates) provided first in the table; outgroup taxa ('raphid pennates') follow after table break. Taxa are listed alphabetically.

**Supplementary fig. S1. Figs A–K.** Cultured *Proschkinia* spp. **Figs A–G.** Epiphytic *Proschkinia* cf. *complanatula* isolated from the central coast of California, USA. **Figs A–C.** Living cells. **Figs A, B.** Valve view. **Fig. C.** Girdle view. **Figs D, E.** Light micrographs showing cleaned valves. **Figs F, G.** Scanning electron micrographs. **Fig. F.** External view of the valve. **Fig. G.** Internal view of the valve. **Fig. H.** Living cells of *P. sulcata* isolated from a loggerhead in Croatia. **Figs I–K.** Living cells of *P. vergostriata* isolated from sea turtles in Florida, USA. **Figs I, J.** Valve view. **Fig. K.** Girdle view. Scale bar: 5 µm.

**Supplementary fig. S2.** Maximum likelihood tree based on the 3-gene dataset (nuclear-encoded ribosomal SSU, chloroplast-encoded *rbcL*, *psbC* markers). Characters representing three categories of bootstrap values from 1000 pseudoreplicates (100%, > 95%, > 70%) over the corresponding nodes. The araphid pennate clades, including the outgroup *Asterionellopsis socialis*, are collapsed in this figure for clarity. The complete tree can be viewed in Supplementary fig. S3.

**Supplementary fig. S3.** Maximum likelihood tree based on the 3-gene dataset (nuclear-encoded ribosomal SSU, chloroplast-encoded *rbcL*, *psbC* markers) with bootstrap values from 1000 pseudoreplicates over the corresponding nodes. The araphid pennate taxon outgroup *Asterionellopsis socialis* was used as the outgroup.

**Supplementary fig. S4.** Strict consensus tree of the 28 most parsimonious trees resulting from the Maximum parsimony analysis of the 3-gene dataset (nuclear-encoded ribosomal SSU, chloroplast-encoded *rbcL*, *psbC* markers) with bootstrap values from 1000 pseudoreplicates over the corresponding nodes. The araphid pennate taxon outgroup *Asterionellopsis socialis* was used as the outgroup.

**Supplementary data S1.** The aligned 3-gene dataset (nuclear-encoded ribosomal SSU, chloroplast-encoded *rbcL*, *psbC* markers) used for the molecular phylogenetic analyses.

## Author contributions

R. Majewska: original concept, drafting and editing manuscript, producing figures, drafting and editing species descriptions, collecting and processing samples, performing microscopy observations and producing LM and SEM images, analysing data; S. Bosak: editing manuscript, drafting and editing species descriptions, collecting and processing samples, performing microscopy observations and producing LM and SEM images, culturing, analysing data; T.A. Frankovich: editing manuscript, drafting and editing species descriptions, collecting and processing samples, performing microscopy observations and producing LM images, analysing data; M.P. Ashworth: editing manuscript, drafting and editing species descriptions, collecting and processing samples, performing microscopy observations

and producing LM and SEM images, culturing, performing molecular and phylogenetic analyses; M.J. Sullivan: editing manuscript, drafting and editing species descriptions; N.J. Robinson: editing manuscript, original concept, providing samples; E.A. Lazo-Wasem: editing manuscript, original concept, providing samples; T. Pinou: editing manuscript, original concept, providing samples; R. Nel: providing access to research station and equipment, organizing fieldwork; S.R. Manning: providing materials and access to research facilities and equipment; B. Van de Vijver: editing manuscript, original concept, processing samples, performing microscopy observations and producing LM and SEM images.

## ORCID

- Roksana Majewska  <http://orcid.org/0000-0003-2681-4304>  
 Sunčica Bosak  <http://orcid.org/0000-0002-4604-2324>  
 Eric A. Lazo-Wasem  <http://orcid.org/0000-0001-5627-1852>

## References

- Anonymous (1975). Proposals for standardization of diatom terminology and diagnoses. *Nova Hedwigia, Beihefte*, **53**: 323–354.
- Archibald, R.E.M. (1983). The diatoms of the Sundays and Great Fish Rivers in the Eastern Cape Province of South Africa. *Bibliotheca Diatomologica*, **1**: 1–362.
- Barinova, S. & Krupa, E. (2017). Bioindication of ecological state and water quality by phytoplankton in the Shardara Reservoir, Kazakhstan. *Environment and Ecology Research*, **5**: 73–92.
- Bjørndal, K.A. (1980). Nutrition and grazing behaviour of the green turtle *Chelonia mydas*. *Marine Biology*, **56**: 147–154.
- Brockmann, C. (1950). Die Watt-Diatomeen der Schleswig-holsteinischen Westküste. *Abhandlungen der Senckenbergischen Naturforschenden Gesellschaft*, **478**: 1–26.
- Brogan, M.W. & Rosowski, J.R. (1988). Frustular morphology and taxonomic affinities of *Navicula complanatoides* (Bacillariophyceae). *Journal of Phycology*, **24**: 262–273.
- Cholnoky, B.J. (1963). Beiträge zur Kenntnis der Ökologie der Diatomeen des Swakop-Flusses in Südwest-Afrika. *Revista Biologica*, **3**: 233–260.
- Clavero i Oms, E. (2009). *Diatomees d'ambients hipersalines costaners. Taxonomía, distribució i emprentes en el registre sedimentari*. Institut d'Estudis Catalans, Barcelona.
- Cox, E.J. (1981). The use of chloroplasts and other features of the living cell in the taxonomy of naviculoid diatoms. In *Proceedings of the 6th Symposium on Recent and Fossil Diatoms* (Ross, R., editor). Otto Koeltz, Koenigstein.
- Cox, E.J. (1988). Taxonomic studies on the diatom genus *Navicula* Bory. V. The establishment of *Parlibellus* gen. nov. for some members of *Navicula* sect. *Microstigmaticae*. *Diatom Research*, **3**: 2–38.
- Cox, E.J. (1998). The identity and typification of some naviculoid diatoms (Bacillariophyta) from freshwater or brackish habitats. *Phycologia*, **37**: 162–175.
- Cox, E.J. (2012). Ontogeny, homology and terminology – wall morphogenesis as an aid to character state definition for pennate diatom systematics. *Journal of Phycology*, **48**: 1–31.
- Ehrlich, A. (1978). The diatoms of the hypersaline Solar Lake (Ne Sinai). *Israel Journal of Botany*, **27**: 1–13.
- Frankovich, T.A., Ashworth, M.P., Sullivan, M.J., Theriot, E.C. & Stacy, N.I. (2018) Epizoic and apochlorotic *Tursiocola* species (Bacillariophyta) from the skin of Florida manatees (*Trichechus manatus latirostris*). *Protist*, **169**: 539–568.
- Frankovich, T.A., Ashworth, M.P., Sullivan, M.J., Vesela, J. & Stacy, N.I. (2016). *Medlinella amphoroidea* gen. et sp. nov. (Bacillariophyta) from the neck skin of loggerhead sea turtles (*Caretta caretta*). *Phytotaxa*, **272**: 101–114.
- Frankovich, T.A., Sullivan, M.J. & Stacy, N.I. (2015). *Tursiocola denysii* sp. nov. (Bacillariophyta) from the neck skin of Loggerhead sea turtles (*Caretta caretta*). *Phytotaxa*, **234**: 227–236.
- Gastineau, R., Kim, S.Y., Lemieux, C., Turmel, M., Witkowski, A., Park, J.G., Kim, B.S., Mann, D.G. & Theriot, E.C. (2019). Complete mitochondrial genome of a rare diatom (Bacillariophyta) *Proschkinia* and its phylogenetic and taxonomic implications. *Mitochondrial DNA Part B*, **4**: 25–26.
- Goloboff, P.A., Farris, J.S. & Nixon, K.C. (2008). TNT, a free program for phylogenetic analysis. *Cladistics*, **24**: 774–786.
- Guillard, R.R.L. (1975). Culture of phytoplankton for feeding marine invertebrates. In *Culture of Marine Invertebrate Animals* (Smith, W.L. & Chanley, M.H., editors). Springer, Boston, MA.
- Hasle, G.R. & Syvertsen, E.E. (1997). Marine diatoms. In *Identifying Marine Phytoplankton* (Tomas, C.R., editor). Academic Press, San Diego, CA.
- Hendey, N.I. (1964). *An Introductory Account of the Smaller Algae of British Coastal Waters. V. Bacillariophyceae (diatoms)*. Reprinted 1976. Otto Koeltz Science Publishers, Koenigstein.
- Hillebrand, H. & Sommer, U. (2000). Effect of continuous nutrient enrichment on microalgae colonizing hard substrates. *Hydrobiologia*, **426**: 185–192.
- Kaleli, A., Krzywda, M., Witkowski, A., Riaux-Gobin, C., Solak, C.N., Zgłobicka, I., Płociński, T., Grzonka, J., Kurzydłowski, K.J., Car, A., Desrosiers, C., Kaska, Y. & McCartney, K. (2018). A new sediment dwelling and epizoic species of *Olifantiella* (Bacillariophyceae), with an account on the genus ultrastructure based on Focused Ion Beam nanocuts. *Fottea*, **18**: 212–226.
- Karayeva, N.I. (1978). Novyj podporyadok diatomovykh vodoroslej (A new suborder of diatoms). *Botanicheskij Zhurnal*, **63**: 1747–1750.
- Karayeva, N.I. & Bukthiyarova, L.N. (2010). Additions to the flora of the Caspian Sea Bacillariophyta. *Algologia*, **20**: 471–481. [in Russian]
- Lange, C.B. & Tiffany, M.A. (2002). The diatom flora of the Salton Sea, California. *Hydrobiologia*, **473**: 179–201.
- Li, C., Ashworth, M., Witkowski, A., Lobban, C.S., Zgłobicka, I., Kurzydłowski, K.J. & Qin S. (2016). Ultrastructural and molecular characterization of diversity among small araphid diatoms all lacking rimoprotulae. I. Five new genera, eight new species. *Journal of Phycology*, **52**: 1018–1036.
- Lobban, C., Scheffer, M., Jordan, R.W., Arai, Y., Sasaki, A., Theriot, E.C., Ashworth, M., Ruck, E.C. & Pennesi, C. (2012). Coral-reef diatoms (Bacillariophyta) from Guam: new records and preliminary checklist, with emphasis on epiphytic species from farmer-fish territories. *Micronesica*, **43**: 237–479.
- Majewska, R., Ashworth, M.P., Lazo-Wasem, E., Robinson, N.J., Rojas, L., Van de Vijver, B. & Pinou, T. (2018a). *Craspedostauros alatus* sp. nov., a new diatom (Bacillariophyta) species found on museum sea turtle specimens. *Diatom Research*, **33**: 229–240.
- Majewska, R., De Stefano, M., Ector, L., Bolanos, F., Frankovich, T.A., Sullivan, M.J., Ashworth, M.P. & Van De Vijver, B. (2017a). Two new epizoic *Achnanthes*

- species (Bacillariophyta) living on marine turtles from Costa Rica. *Botanica Marina*, **60**: 303–318.
- Majewska, R., De Stefano, M. & Van De Vijver, B. (2018b). *Labellicula lecohuiana*, a new epizoic diatom species living on green turtles in Costa Rica. *Nova Hedwigia, Beihefte*, **146**: 23–31.
- Majewska, R., Kociolek, J.P., Thomas, E.W., De Stefano, M., Santoro, M., Bolanos F. & Van De Vijver, B. (2015a). *Chelonicola* and *Poulinea*, two new gomphonemoid diatom genera (Bacillariophyta) living on marine turtles from Costa Rica. *Phytotaxa*, **233**: 236–250.
- Majewska, R., Santoro, M., Bolanos, F., Chaves, G. & De Stefano, M. (2015b). Diatoms and other epibionts associated with olive ridley (*Lepidochelys olivacea*) sea turtles from the Pacific coast of Costa Rica. *PLoS ONE*, **10**: e0130351. doi: [10.1371/journal.pone.0130351](https://doi.org/10.1371/journal.pone.0130351).
- Majewska, R., Van De Vijver, B., Nasrolahi, A., Ehsanpour, M., Afkhami, M., Bolanos, F., Iamunno, F., Santoro, M. & De Stefano, M. (2017b). Shared epizoic taxa and differences in diatom community structure between green turtles (*Chelonia mydas*) from distant habitats. *Microbial Ecology*, **74**: 969–978.
- Majewska, R., Ashworth, M.P., Lazo-Wasem, E., Robinson, N.J., Rojas, L., Van de Vijver, B. & Pinou, T. (2018a). *Craspedostauros alatus* sp. nov., a new diatom (Bacillariophyta) species found on museum sea turtle specimens. *Diatom Research*, **33**: 229–240.
- Majewska, R., De Stefano, M. & Van De Vijver, B. (2018b). *Labellicula lecohuiana*, a new epizoic diatom species living on green turtles in Costa Rica. *Nova Hedwigia, Beihefte*, **146**: 23–31.
- Mejdandžić, M., Bosak, S., Nakov, T., Ruck, E., Orlić, S., Udovič, M.G., Peharec Štefanić, P., Špoljarić, I., Mršić, G. & Ljubešić, Z. (2018). Morphological diversity and phylogeny of the diatom genus *Entomoneis* (Bacillariophyta) in marine plankton: six new species from the Adriatic Sea. *Journal of Phycology*, **54**: 275–298.
- Nawrocki, E.P. (2009). *Structural RNA Homology Search and Alignment using Covariance Models*. Washington University, St. Louis, MI.
- Nixon, K. (2002). Winclada ver. 1.00.08. Published by the author. Ithaca, NY. <http://www.diversityoflife.org/winclada/>.
- Pezzolesi, L., Pichierri, S., Samori, C., Totti, C. & Pistocchi, R. (2017). PUFAs and PUAs production in three benthic diatoms from the northern Adriatic Sea. *Phytochemistry*, **142**: 85–91.
- Pichierri, S., Accoroni, S., Pezzolesi, L., Guerrini, F., Romagnoli, T., Pistocchi, R. & Totti, C. (2017). Allelopathic effects of diatom filtrates on the toxic benthic dinoflagellate *Ostreopsis cf. ovata*. *Marine Environmental Research*, **131**: 116–122.
- Riaux-Gobin, C., Witkowski, A., Chevallier, D. & Daniszewska-Kowalczyk, G. (2017a). Two new *Tursiocola* species (Bacillariophyta) epizoic on green turtles (*Chelonia mydas*) in French Guiana and Eastern Caribbean. *Fottea*, **17**: 150–163.
- Riaux-Gobin, C., Witkowski, A., Kociolek, J.P., Ector, L., Chevallier, D. & Compere, P. (2017b). New epizoic diatom (Bacillariophyta) species from sea turtles in the Eastern Caribbean and South Pacific. *Diatom Research*, **32**: 109–125.
- Rivera, S.F., Vasselon, V., Ballorain, K., Carpentier, A., Wetzel, C.E., Ector, L., Bouchez, A. & Rimet, F. (2018). DNA metabarcoding and microscopic analyses of sea turtles biofilms: Complementary to understand turtle behavior. *PLoS ONE*, **13**: e0195770. doi: [10.1371/journal.pone.0195770](https://doi.org/10.1371/journal.pone.0195770).
- Riznyk, R.A. (1973). Interstitial diatoms from two tidal flats in Yaquina Estuary, Oregon, USA. *Botanica Marina*, **16**: 113–138.
- Robinson, N.J., Majewska, R., Lazo-Wasem, E., Nel, R., Paladino, F.V., Rojas, L., Zardus, J.D. & Pinou, T. (2016). Epibiotic diatoms are universally present on all sea turtle species. *PLoS ONE*, **11**: e0157011. doi: [10.1371/journal.pone.0157011](https://doi.org/10.1371/journal.pone.0157011).
- Ross, R., Cox, E.J., Karayeva, N.I., Mann, D.G., Paddock, T. B.B., Simonsen, R. & Sims, P.A. (1979). An amended terminology for the siliceous components of the diatom cell. *Nova Hedwigia, Beihefte*, **64**: 513–533.
- Ross, R. & Sims, P.A. (1972). The fine structure of the frustule in centric diatoms: a suggested terminology. *British Phycological Journal*, **7**: 139–163.
- Round, F.E., Crawford, R.M. & Mann, D.G. (1990). *The Diatoms: Biology and Morphology of the Genera*. Cambridge University Press, Cambridge.
- Sabir, J.S.M., Theriot, E.C., Manning, S.R., Al-Malki, A.L., Khiyami, M.A., Al-Ghamdi, A.K., Sabir, M.J., Romanovicz, D.K., Hajrah, N.H., El Omri, A., Jansen, R.K. & Ashworth, M.P. (2018). Phylogenetic analysis and a review of the history of the accidental phytoplankton, *Phaeodactylum tricornutum* Bohlin (Bacillariophyta). *PLoS ONE*, **13**: e0196744. doi: [10.1371/journal.pone.0196744](https://doi.org/10.1371/journal.pone.0196744).
- Sempere-Valverde, J., Ostalé-Valriberas, E., Farfán, G.M. & Espinosa, F. (2018). Substratum type affects recruitment and development of marine assemblages over artificial substrata: a case study in the Alboran Sea. *Estuarine, Coastal and Shelf Science*, **204**: 56–65.
- Simonsen, R. (1987). *Atlas and Catalogue of the Diatom Types of Friedrich Hustedt*, volumes 1–3. J. Cramer, Berlin.
- Stamatakis, A. (2014). RAxML Version 8: a tool for phylogenetic analysis and post-analysis of large phylogenies. *Bioinformatics*, **30**: 1312–1313.
- Theriot, E.C., Ashworth, M.P., Nakov, T., Ruck, E.C. & Jansen, R.K. (2015). Dissecting signal and noise in diatom chloroplast protein encoding genes with phylogenetic information profiling. *Molecular Phylogenetics and Evolution*, **89**: 28–36.
- Underwood, G.J.C. & Yallop, M.L. (1994). *Navicula pargemina* sp. nov. – a small epipelagic species from the Severn Estuary, U.K. *Diatom Research*, **9**: 473–478.
- van der Werff, A. (1955). A new method of concentrating and cleaning diatoms and other organisms. *Verhandlungen der Internationalen Vereinigung der Limnologie*, **2**: 276–277.
- Witkowski, A., Lange-Bertalot, H. & Metzeltin, D. (2000). Diatom flora of marine coasts 1. *Iconographia Diatomologica*, **7**: 1–925.
- Zardus, J.D. & Hadfield, M.G. (2004). Larval development and complemental males in *Chelonibia testudinaria*, a barnacle commensal with sea turtles. *Journal of Crustacean Biology*, **24**: 409–421.
- Zgrundo, A., Lemke, P., Pniewski, F., Cox, E.J. & Latała, A. (2013). Morphological and molecular phylogenetic studies on *Fistulifera saprophila*. *Diatom Research*, **28**: 431–443.